

# Two-dimensional layered materials for modifying solid-state electrolytes in lithium batteries via interface engineering

Shuoguo Yuan <sup>\*</sup>, Qian Xia, Can Huang, Hongyun Jin <sup>\*</sup>

Faculty of Materials Science and Chemistry, China University of Geosciences, Wuhan 430074, China



## ARTICLE INFO

**Keywords:**

Two-dimensional materials  
Solid-state electrolytes  
Lithium batteries  
Interface engineering

## ABSTRACT

Lithium-ion batteries have been widely used in mobile electronic devices and electric vehicles, but the safety issues of lithium-ion batteries have become increasingly prominent owing to the risk of leak out and explosion with liquid electrolytes. Solid-state electrolytes (SSEs) with high ionic conductivity and low cost are considered as one of the most attractive alternatives to replacing liquid electrolytes. However, the poor interfacial compatibilities of SSE in lithium batteries lead to the failure, which severely hinders their development. Recent studies have shown that two-dimensional (2D) layered materials can improve the interface stability of SSE to lithium metal. In this Review, we will mainly introduce the fundamentals of SSEs and interface issues, and then summarize 2D materials-based modification strategy for SSEs. Recent advances have been highlighted in the aspects of using 2D materials for improving the interface of SSEs, which are very promising for energy applications. The availability of the 2D materials offers a rich playground, which not only improves the electrochemical performance of solid-state lithium batteries, but also conceives deep understanding the mechanism of interface modulation. Lastly, the perspective is provided to address the current challenges and issues of SSEs in lithium batteries.

## 1. Introduction

With the widespread application of electric vehicles, the safety issues of lithium-ion batteries as the energy source of electric vehicles have become increasingly prominent. Traditional lithium-ion batteries are usually composed of liquid electrolytes, which help lithium-ion to and from the cathode and anode [1,2]. However, these liquid electrolytes also have serious safety problems, because the liquid organic solvents used in these electrolytes are flammable and have the risk of leakage [3]. In addition, the growth of lithium dendrites in liquid lithium-ion batteries is an inevitable problem, which causes short circuit of the battery and then leads to explosion [4]. Liquid lithium-ion batteries also limit the use of high-voltage cathode materials and the realization of high energy density batteries. Based on these problems, liquid lithium-ion batteries urgently need to be further developed and improved. More and more attention has been paid to the replacement of liquid lithium-ion batteries with all solid-state batteries with lithium metal anodes. Solid-state batteries can completely resolve the safety problem of liquid lithium-ion batteries and achieve a battery system with higher specific energy, which is expected to be widely used in large power storage

systems such as electric vehicles and electronic equipment [5]. SSEs, as the core component in solid-state batteries, should have high ionic conductivity, negligible electronic conductivity, stable chemistry, wide electrochemical window, good interfacial compatibility to move toward commercialization in batteries, and these properties simultaneously is still difficult to achieve [6].

Typically, most SSEs have room temperature ionic conductivity up to  $10^{-3}$  S cm<sup>-1</sup>, but it is lower compared to liquid electrolytes  $10^{-2}$  S cm<sup>-1</sup>, which limits the specific capacity of active materials during charging and discharging [7]. Secondly, with the application of lithium metal anodes, the interfacial side reactions between the electrode and electrolyte are intensified, which leads to the failure of lithium anodes. In addition, at high current densities, the depletion of anions in the electrolyte near the anode generates a space charge that drives a hydrodynamic instability called electric convection. This electric convection attracts ions from the surrounding area of the growing dendrite and concentrates them at the top of the dendrite, thus promoting dendrite growth [8]. Interfacial issues are prevalent at the interfaces between different ionic conductors throughout the cell system. For example, the interfaces between electrode/SSE, inorganic/polymer SSE multilayer,

\* Corresponding authors.

E-mail addresses: [yuanshuoguo@cug.edu.cn](mailto:yuanshuoguo@cug.edu.cn) (S. Yuan), [jinhongyun@cug.edu.cn](mailto:jinhongyun@cug.edu.cn) (H. Jin).

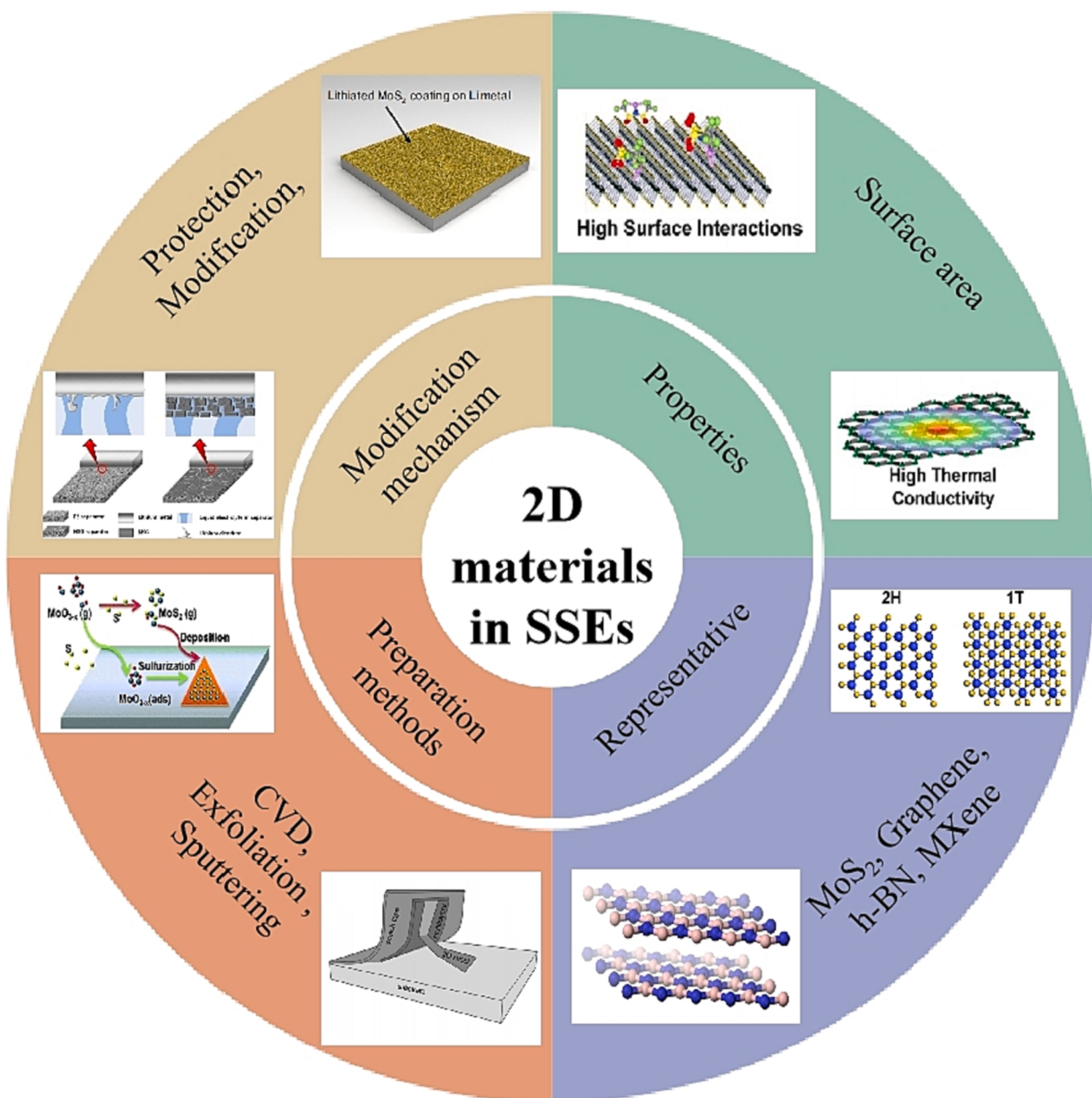


**Fig. 1.** Properties, preparation methods and modification mechanisms of common 2D materials [14]. Copyright 2020, American Chemical Society [15]. Copyright 2017, Royal Society of Chemistry [16]. Copyright 2018, Elsevier [17]. Copyright 2015, Royal Society of Chemistry [18]. Copyright 2015, American Chemical Society [19]. Copy 2018, Springer Nature.

electrode/buffer layer and SSE/buffer layer all have interfacial charge transfer resistance, which is caused by large volume changes of electrodes during cycling, lattice mismatch, leading to poor mechanical integrity, chemical instability and electrochemical incompatibility [9]. For these reasons, the interfacial impedance of solid-state lithium batteries may be two to three orders of magnitude higher than that of lithium-ion batteries containing organic electrolytes, and this value may also increase dramatically during long-term cycling and significantly impede the cycle life of the battery [10]. Therefore, the electrolyte-electrode interface issue has become a major challenge for solid-state lithium metal batteries.

Various advanced materials and structures have been developed in recent years to resolve the interface problem in all-solid-state lithium-metal batteries and further improve the electrochemical performance of the batteries. Among these advanced materials, 2D layered materials consisting of a single layer of atoms have become a prominent research topic due to their excellent properties [11]. Firstly, 2D materials have

good chemical stability and mechanical strength, which are beneficial to mitigate the interfacial side reactions between electrolyte and lithium metal anode and inhibit the growth of lithium dendrites, thus prolonging the battery life [12]. Secondly, the high specific surface area of 2D materials provides a large number of active sites for lithium-ion transport, which helps to promote the transport of lithium-ion [13]. In addition, 2D materials have a significant role in suppressing the shuttle effect of sulfides in Li/S batteries and in enhancing the ionic conductivity of solid polymer electrolytes. In recent years, the use of 2D materials to modify the interface of solid-state lithium-metal batteries has become increasingly remarkable and is expected to be a key material for solving the interface problems of all-solid-state lithium-metal batteries [14]. In this Review, we will mainly introduce the fundamentals of SSEs including inorganic solid-state electrolytes (ISEs), solid polymer electrolytes (SPEs), composite solid-state electrolytes (CSEs), and then we summarize 2D materials-based modification strategy for SSEs. Recent advances have been highlighted in the aspects of using 2D materials for

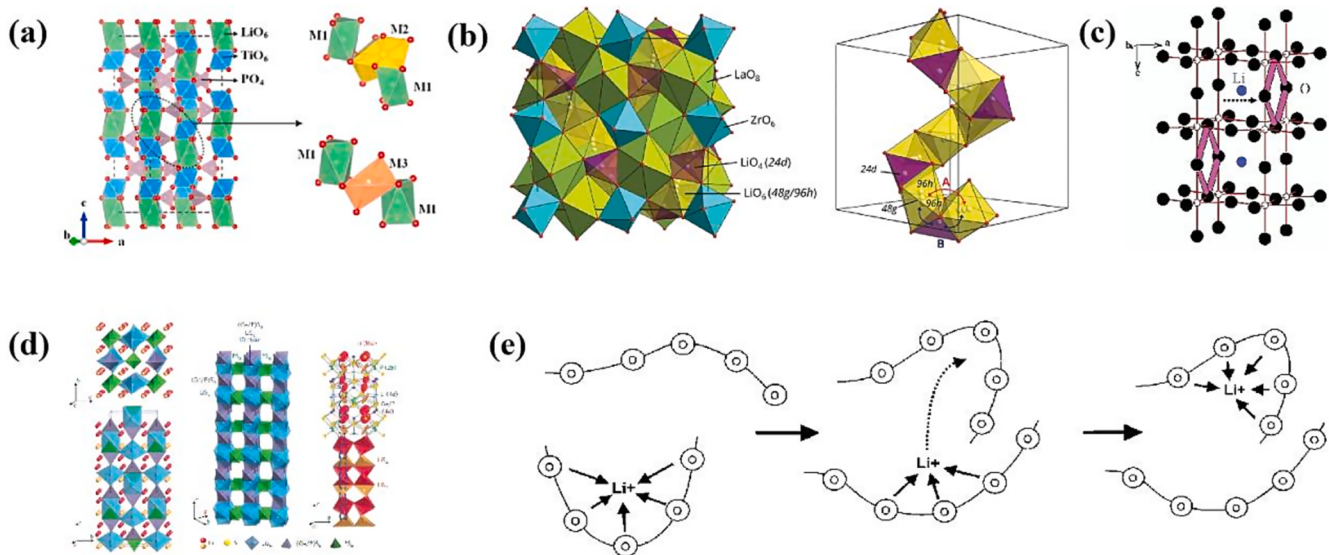


**Fig. 2.** (a) Crystal structure of  $\text{LiTi}_2(\text{PO}_4)_3$ , M1, M2 and M3 sites of Li atoms, and the migration pathway in  $\text{LiTi}_2(\text{PO}_4)_3$  [25]. Copyright 2019, Elsevier. (b) Crystal Structure of Cubic LLZO and Wyckoff positions of the  $\text{Li}^+$ . The centers of tetrahedral and octahedral sites are noted as 24d and 48 g sites, respectively, and the 96 h sites are slightly displaced off the 48 g sites.  $\text{LiO}_6$  and  $\text{LiO}_4$  connection and the two possible Li migration pathways [32]. Copyright 2019, Royal Society of Chemistry. (c) Schematic structure of  $\text{Li}_{3x}\text{La}_{(2/3-x)}\text{TiO}_3$  showing the bottleneck for the  $\text{Li}^+$  ion migration. The Li, La, and vacancy are distributed at A sites [35]. Copyright 2003, American Chemical Society. (d) Crystal structure of LGPS, one-dimensional view of LGPS and  $\text{Li}^+$  transport pathway [39]. Copyright 2011, Springer Nature. (e) Schematic of the segmental motion assisted diffusion of  $\text{Li}^+$  in the PEO matrix. The circles represent the ether oxygens of PEO [42]. Copyright 1998, John Wiley and Sons.

improving the interface of SSEs and their mechanisms (Fig. 1), providing directions for the development of 2D materials in SSEs. The availability of the 2D materials offer a rich playground for not only improving the electrochemical performance of solid-state lithium batteries, but also conceiving deep understanding the mechanism of interface modulation, which are very promising for energy, electronic, and optoelectronic applications.

## 2. Structure and properties of SSE

Currently, SSEs mainly include ISEs, SPEs, and CSEs [20]. ISEs include oxide SSEs, sulfide SSEs, borohydride SSEs, and halide SSEs, among which oxide SSEs and sulfide SSEs are the most popular materials for researchers due to their unique advantages [21]. SPEs and SPEs also have properties not found in ISEs and are widely used in solid-state batteries [22]. This section introduces the structures and properties of these major SSEs, and provides theoretical support for the modification of 2D materials on SSEs.

### 2.1. Structure information

#### 2.1.1. Oxide-based SSEs

NASICON-type electrolytes was first reported by Goodenough in 1976 [23], and the chemical formula was  $\text{LiM}_2(\text{PO}_4)_3$ . The M-site was usually occupied by four valence cations such as Ge, Zr, Ti, Sn, etc. Aono et al. found that partial  $\text{Ti}^{4+}$  doping with trivalent cations ( $\text{Al}^{3+}$ ,  $\text{Sc}^{3+}$ ,  $\text{Ga}^{3+}$ ,  $\text{Fe}^{3+}$ , etc.) resulted in a great increase in ionic conductivity [24]. In general, the NASICON-type electrolytes skeleton is rhombic structure, and the space group is R-3C. Take  $\text{Li}_{1+x}\text{Al}_x\text{Ti}_{2-x}(\text{PO}_4)_3$  (LATP,  $0 \leq x \leq 0.5$ ) as an example, as shown in Fig. 2a [25]. When  $x = 0$ , in  $\text{LiTi}_2(\text{PO}_4)_3$ ,  $\text{TiO}_6$  octahedron and  $\text{PO}_4$  tetrahedron are connected at the same vertex to form a three-dimensional skeleton. Each  $\text{TiO}_6$  octahedron is connected to six  $\text{PO}_4$  tetrahedrons, and each  $\text{PO}_4$  tetrahedron is connected to four  $\text{TiO}_6$  octahedrons.  $\text{Li}^+$  completely occupies the M1 site. When  $x > 0$ ,  $\text{Ti}^{4+}$  is replaced by partially introduced  $\text{Al}^{3+}$ , which is distributed on the position of  $\text{TiO}_6$  octahedron Ti before. In addition, equal molar amount of  $\text{Li}^+$  is introduced, which occupies the M2 site. The connection

between M1 and M2 constitutes the  $\text{Li}^+$  transmission channel [26]. In addition, doped  $\text{Al}^{3+}$  can reduce the strength of Li-O bond, enhance the Ti-O bond, and promote the transport of  $\text{Li}^+$  in LATP.  $\text{Li}^+$  is transported in a three-dimensional structure framework composed of  $[\text{Ti}/\text{Al}]_6$  octahedron and  $\text{PO}_4$  tetrahedron, which has good conductivity [27].

Garnet-type electrolytes has been widely concerned in the field of electrochemical energy storage technology because of its high ionic conductivity, good thermal stability, good chemical stability with lithium metal, wide electrochemical window and other advantages [28]. Thangadurai et al. first reported a new fast lithium-ion conductor  $\text{Li}_5\text{La}_3\text{M}_2\text{O}_{12}$  (M = Nb, Ta) with garnet like structure in 2003, but its ionic conductivity was low ( $\sim 10^{-6} \text{ S cm}^{-1}$  at  $25^\circ\text{C}$ ), and the activation energy did not exceed 0.6 eV [29]. Several years later, Murugan et al. developed a new garnet-type electrolyte  $\text{Li}_7\text{La}_3\text{Zr}_2\text{O}_{12}$  (LLZO) containing zirconium by doping with Zr instead of M sites, with an increased ionic conductivity of  $2.44 \times 10^{-4} \text{ S cm}^{-1}$ , and an activation energy as low as 0.31 eV [30]. The structure of garnet-type electrolytes was generally  $\text{A}_3\text{B}_3\text{C}_2\text{O}_{12}$  (A for Ca, Mg, Y, La or rare earth element, B for Si, Ge or Al, and C for Al, Fe, Ga, Ge, Mn, Ni or V). In crystallography, it contained three different types of cation coordination environments, in which A, B and C cations had eight, four and six coordination sites respectively. The 24d-A tetrahedral site constituted a three-dimensional connecting gap space in the  $\text{B}_3\text{C}_2\text{O}_{12}$  framework, which was bridged by a single octahedron that has a relative common surface with the adjacent 24d-A site, and the A-site, a dodecahedral gap in the skeleton, which was usually occupied by a cation with a large ionic radius. Since La had the largest ionic radius among the rare earth elements, it was the most suitable element for the formation of the A-site [31]. LLZO adopts two different crystal structures-tetragonal (t-LLZO) and cubic (c-LLZO), Fig. 2b displays the crystal structure of c-LLZO, consisting of 8-fold coordination of the dodecahedral  $\text{LaO}_8$  (24c) and 6-fold coordination octahedral  $\text{ZrO}_6$  (16a), with Li atoms located in interstitial positions in tetrahedral 24d sites and octahedral 48 g or eccentric 96 h sites, resulting in the displacement of Li ions from the central 48 g site to the eccentric 96 h site within the octahedron due to Li-Li repulsion interactions [32].

Perovskite-type electrolytes has high ionic conductivity, good thermal stability and mechanical properties, which is considered as a

promising candidate material for SSE [33]. The most important perovskite-type lithium lanthanum titanate SSE was developed by Inaguma et al. in 1993 [34], and the general formula can be expressed as  $\text{Li}_{3x}\text{La}_{(2/3)-x}\text{TiO}_3$  (LLTO). The  $x$  value was  $0.07 \sim 0.13$ , the activation energy was  $0.3 \sim 0.4$  eV, and the bulk conductivity was as high as  $1 \times 10^{-3} \text{ S cm}^{-1}$ , but due to the high grain boundary resistance, the total conductivity in the battery was low ( $\sim 2 \times 10^{-5} \text{ S cm}^{-1}$ ). The crystal structure of LLTO is shown in Fig. 2c [35], Li and La ions occupy the central A position, while Ti ions occupy the angular B position. Oxygen ions form a bottleneck, causing potential obstacles for lithium-ion to migrate from one A point to the adjacent A point.

### 2.1.2. Sulfide-based SSEs

The study of sulfide electrolytes originated in the early 1900s. Compared with oxide electrolytes, sulfide SSEs have higher ionic conductivity because of the large ionic radius of sulfur, low electronegativity, and high polarization ability, which increases the concentration of free lithium-ion by weakening the bonding between lithium-ion and adjacent skeletal structures while building larger lithium-ion transport channels [36]. In addition, the sulfide SSEs has a soft texture and low interfacial impedance between the electrolyte and the electrode, achieving an ionic conductivity comparable to that of the liquid electrolyte [37]. Common types of sulfide electrolytes in ceramic crystalline form include Thio-LISION type, sulfur silver germanite type, and  $\text{Li}_{10}\text{GeP}_2\text{S}_{12}$ -type [38]. For sulfide electrolytes, despite their high ionic conductivity at room temperature, they have extremely poor stability and tend to react with humid air environments, making their preparation and preservation processes harsh and difficult to put into mass production. For example,  $\text{Li}_{10}\text{GeP}_2\text{S}_{12}$ -type SSEs (crystal structure shown in Fig. 2d will react with lithium metal electrodes to form SSE films during cycling, and the resulting Li-Ge alloy will increase the electronic conductivity of the electrolyte and increase the interfacial instability [39].

### 2.1.3. Polymer-based SSEs

As early as the 1970s, Wright et al. discovered ion-conducting complexes between polyethylene oxide (PEO) and alkali metal salts, opening up a new direction in the study of SPEs [40]. Unlike crystalline ISEs, SPEs are highly flexible and can be applied to any cell shape, in addition to improved safety and stability. However, most polymer electrolytes, such as PEO, polyvinylidene fluoride (PVDF), and polyacrylonitrile (PAN), have significantly lower ionic conductivity than inorganic oxide SSEs and liquid electrolytes [41]. Among them, PEO has become the most studied polymer electrolyte body due to its good mechanical properties and good compatibility with electrodes. It is able to dissolve a variety of salts through its ether-oxygen bonding interaction with cations and is used in a stand-alone form for all-solid-state battery design. Fig. 2e presents the transport mechanism of lithium- ion in SPEs using PEO as an example, where lithium-ion pass through the PEO matrix segmented motion between the complex sites, complexing with approximately five ether oxygens of the PEO chain, greatly reducing the mobility of the cation [42]. Because of this, the tight chain stacking in the highly crystalline PEO makes it impossible to transport lithium-ion effectively, limiting its ionic conductivity and lithium-ion mobility number. The conductivity of PEO-based SSEs is only  $10^{-7} \text{ S cm}^{-1}$  at room temperature, which is far below the requirement for normal operation of lithium batteries [43,44]. This is usually done by increasing the crystallinity of PEO and elevating the temperature above the glass transition temperature. This accelerates the chain segment motion to promote ion transport and facilitates the dissociation of lithium salts, where bis(trifluoromethanesulfonyl)imide (LiTFSI) has a flexible anion TFSI<sup>-</sup>, which facilitates the reduction of PEO chain crystallinity and exhibits excellent thermal, chemical and electrochemical stability, but the mechanical strength and stability of the electrolyte are somewhat reduced [45]. Through the design of the polymer structure, it is possible to decouple the Li<sup>+</sup> transport from the chain segment motion of the polymer [46].

And in order to realize the dissolution of lithium salts as well as the dissociation of anions and cations, the polar groups in the polymer must have strong ion-dipole interactions with Li<sup>+</sup>, but this will also hinder the Li<sup>+</sup> transport. Therefore, appropriate coordination structures and moderate interaction strengths are the basis for rapid Li<sup>+</sup> transport in SPEs [47]. The high degree of designability of the polymer molecular structure offers great possibilities for designing SPEs with high ionic conductivity. Hu et al. reported a series of imidazoline-containing crystalline ionic covalent organic frameworks as mono-ionic conducting covalent organic frameworks solid electrolyte materials, in which Li<sup>+</sup> can be freely transported through the intrinsic channels with excellent ionic conductivity (up to  $7.2 \times 10^{-3} \text{ S cm}^{-1}$ ) and an impressively low activation energy (down to 0.10 eV). These properties are attributed to the weak binding interactions of Li<sup>+</sup> with imidazolates and the porous 2D framework structure of such ionic covalent organic frameworks, which differs from the common ion transport driven by fragmentation motion by establishing unique Li<sup>+</sup> transport channels that are expected to accelerate the Li<sup>+</sup> transport in the SPE [48]. On the other hand, the high interfacial contact between SPE and electrode may become an important factor affecting the battery performance. In order to minimize the interfacial impedance of SPE/electrode, a buffer layer or a modification layer can be formed on the surface of the electrode by physical and chemical in situ polymerization methods to improve the interfacial compatibility and ion transport of SPE/electrode [49,50]. In addition, the narrow electrochemical window of SPE reduces its stability at the cathode. To improve the electrochemical window, appropriate polymer structures, lithium salts, and additives must be designed, and the effect of interactions between components in SPE on the oxidation window should also be considered. Yang et al. prepared poly(1,3-dioxolane) (PDOL) solid electrolyte membranes for the first time by a rapid surface-initiated 1,3- dioxolane (DOL) polymerization process with the interaction of the substrate and the initiator. The PDOL electrolyte has a high electrochemical stabilization window up to 5.0 V and can be friendly to various cathodic environments, including sulfur and LiFePO<sub>4</sub> (LFP), LiCoO<sub>2</sub> and LiNi<sub>0.6</sub>Co<sub>0.2</sub>Mn<sub>0.2</sub>O<sub>2</sub> (NMC622) [51]. Subsequently, Yang et al. reported a highly homogeneous poly(1,3-dioxolane) CSE film with an electrochemical window of more than 4.9 V through the in situ catalytic polymerization effect of yttria-stabilized zirconia nanoparticles on the polymerization of DOL [52]. Finally, it is necessary for researchers to have a deeper understanding of the behavior of the SPEs on the lithium-metal surface and the deposition principle, to solve the problem of SPE reaction with strongly reducing lithium, and to add suitable fillers to obtain SPEs with high safety, high mechanical strength, and high ionic conductivity.

### 2.1.4. Composite SSEs

CSEs are prepared by combining the advantages of different types of SSEs, such as the high ionic conductivity of ISEs and the flexibility of SPEs [53]. Depending on the content of inorganic and polymer components in the electrolyte, CSEs can be divided into two categories: inorganic components used as fillers for compounding with polymers/lithium salts (ceramics in polymers), or polymer/lithium salts used as fillers added to ISEs (polymers in ceramics) [54]. The introduction of a certain amount of inorganic inert fillers into the polymer matrix can improve the amorphous ratio of the polymer, lower the melting point and glass transition temperature of the polymer matrix, promote lithium-ion migration, improve lithium-ion conductivity and the mechanical properties and heat resistance of the electrolyte. Besides, active fillers represented by ISEs can also be applied in high energy density lithium batteries [55]. The active materials can provide additional lithium-ion transport channels, exhibit high lithium-ion conductivity and excellent electrochemical properties, and also significantly improve the solid composite electrolytes through interactions with the polymer matrix, such as ionic dipoles, hydrogen bonding, p-p bonding, Lewis acid-base theory, electrochemical stability window, lithium-ion migration number, interfacial contact and inhibition of lithium dendrites [41].

**Table 1**  
Properties of the main SSEs.

SSE		Typical materials	Ionic conductive (S cm <sup>-1</sup> )	Stability	Other properties	Ref
Oxide	NASICON	Li <sub>1+x</sub> Al <sub>x</sub> Ti <sub>2-x</sub> (PO <sub>4</sub> ) <sub>3</sub> , Li <sub>1.5</sub> Al <sub>0.5</sub> Ge <sub>1.5</sub> (PO <sub>4</sub> ) <sub>3</sub>	10 <sup>-4</sup> ~ 10 <sup>-3</sup>	Stable to air, Unstable to lithium metal	High interface impedance, Growth Li dendrites	[56,57]
	Garnet	Li <sub>5</sub> La <sub>3</sub> M <sub>2</sub> O <sub>12</sub> (M = Nb,Ta), Li <sub>7</sub> La <sub>3</sub> Zr <sub>2</sub> O <sub>12</sub> , Li <sub>6.5</sub> La <sub>3</sub> Zr <sub>0.5</sub> Ta <sub>1.5</sub> O <sub>12</sub>	10 <sup>-4</sup> ~ 10 <sup>-3</sup>	Stable to lithium metal, Unstable to air	High mechanical strength, Wide electrochemical window	[58–60]
	Perovskite	Li <sub>3x</sub> La <sub>(2/3)-x</sub> TiO <sub>3</sub> , La <sub>0.5</sub> Li <sub>0.5</sub> TiO <sub>3</sub>	10 <sup>-3</sup> (bulk) 10 <sup>-4</sup> (total)	Stable to air, Unstable to lithium metal	High volume conductivity, High resistance of crystal	[61,62]
Sulfide		Li <sub>10</sub> GeP <sub>2</sub> S <sub>12</sub> , Li <sub>2</sub> S-P <sub>2</sub> S <sub>5</sub>	10 <sup>-4</sup> ~ 10 <sup>-2</sup>	Unstable to air and lithium metal	Limited electrochemical window, Formation of space charge layer	[63]
Polymer		PEO, PAN, PVDF	10 <sup>-8</sup> ~ 10 <sup>-4</sup>	Stable to air and lithium metal	Flexible, Formation of passivation layer	[64,65]
Composite		PEO-LATP, PEO-Al <sub>2</sub> O <sub>3</sub>	10 <sup>-5</sup> ~ 10 <sup>-4</sup>	Poor interface stability	Good processability, High mechanical strength	[66]

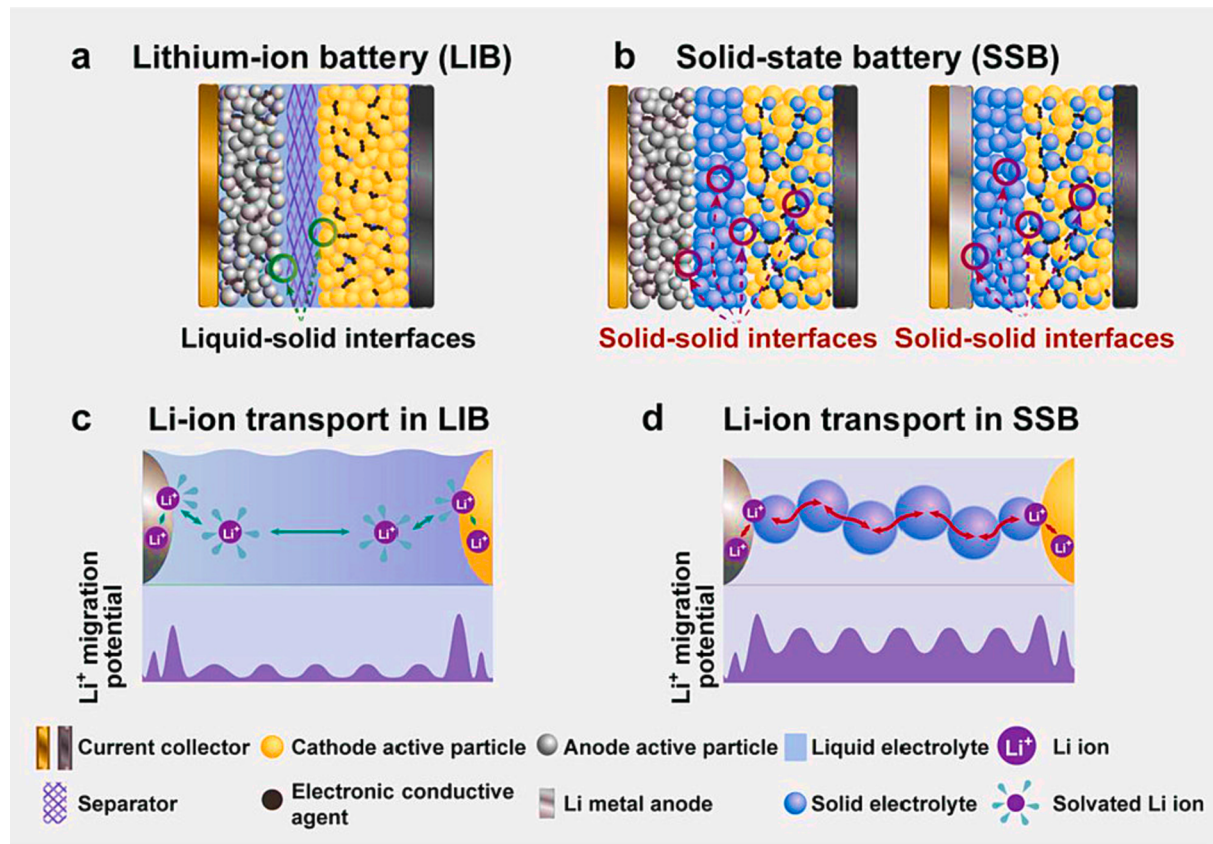


Fig. 3. Change from liquid-solid interface to solid-solid interface [68]. Copyright 2022, John Wiley and Sons.

## 2.2. Physical and chemical properties

As the core component of all solid-state lithium battery, SSE has the characteristics of non-flammability, wide electrochemical window, good thermal stability, etc., which is safer and higher energy density than traditional organic electrolyte lithium-ion battery. In addition, the SSE can also replace the traditional separator, making the battery miniaturized, and has broad application prospects in wearable batteries. In recent decades, a large number of materials have been studied experimentally and theoretically as potential SSE candidate materials, such as NASICON, perovskite, garnet, sulfide, polymer, composite, etc. Table 1 summarizes the main physical and chemical properties of these SSEs.

## 3. Interface engineering methods

The substitution of SSE for liquid electrolyte inevitably introduces a large number of solid interfaces in solid-state batteries. A thorough understanding of the role of these interfaces is a necessary condition to reasonably optimize the performance of solid-state batteries. Compared with liquid electrolytes, SSEs do not have wettability, and most of them are heterogeneous [67]. They may also show different types of “internal interfaces”, such as grain boundaries in polycrystalline SSEs, interfaces between inorganic fillers and polymer matrix in CSEs, and interfaces between crystal regions and polymer matrix [68]. The properties of these interfaces are very different from those of liquid-solid interfaces, it

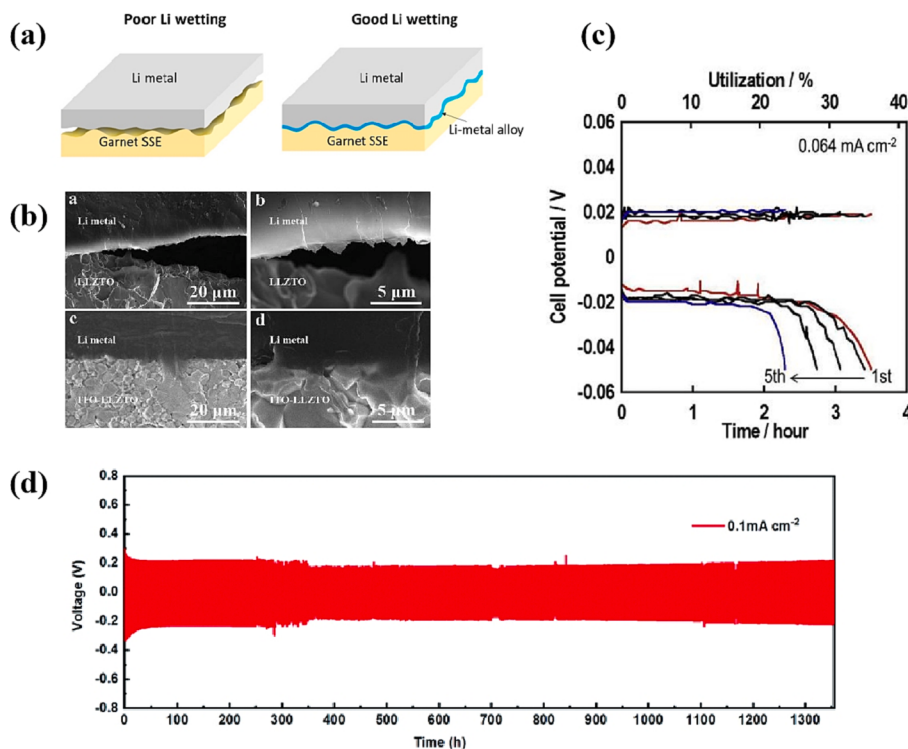


**Fig. 4.** (a) Schematic of engineered garnet SSE/Li interface using Li-metal alloy [83]. Copyright 2017, Authors. (b) Cross-sectional scanning electron microscopy images of the Li/LLZTO interface without and with an ITO interlayer [84]. Copyright 2020, Elsevier. (c) Galvanostatic cycling tests for the Li symmetric cell inserting Au thin films [87]. Copyright 2016, Elsevier. (d) Galvanostatic cycling for the lithium plating/stripping measurement in Li-Li symmetrical cell with PPE-15 wt% based on a current density of  $0.10 \text{ mA cm}^{-2}$  at  $40^\circ\text{C}$  [89]. Copyright 2019, Royal Society of Chemistry.

is often the bottleneck of ion transport in solid-state batteries (Fig. 3). For example, the formation of grain boundaries and space charge layers in ISEs, the charge transfer reaction at the interface in SPEs, the formation and transformation of the passivation layer on the lithium electrode surface, and the interface contact between different phases in CSEs has a great impact on the electrochemical performance of the cell, such as the cycle life, coulomb efficiency, voltage efficiency, etc [69]. In view of various interface challenges between SSE and electrode materials, researchers have proposed a variety of strategies to improve the interface stability. On the positive side, due to the poor wettability of SSE to the positive electrode, the interface modification layer is mainly introduced to reduce the interface resistance and inhibit the formation of space charge layer [70,71]. For SPE, it can also be modified to improve the upper limit of its electrochemical window [72]. On the negative side, there are mainly lithium dendrite growth and interface side reactions. The interface of the negative side can be optimized by modifying the interface and introducing artificial SSE film [73].

Lithium metal is considered to be the key material to realize high energy density battery due to its outstanding performance, while lithium metal as anode electrode material also has problems such as unstable contact with electrolyte and easy to produce lithium dendrites. Currently, researchers mainly use adding interface layer and adjusting electrolyte composition to resolve the problem of anode electrode interface side [9]. And there are many strategies to optimize SSE in contact with lithium anode for high energy density and practical applications [74,75]. The conductivity of SSE is affected by carrier concentration, migration energy barrier and crystal structure. In general, the conductivity is maximized when the carrier concentration reaches an optimal level with both abundant carriers and free hopping sites [76]. The ion migration distance can be shortened and accelerated by adjusting the thickness of the ISE [77]. The addition of nanofillers to SPEs is also a direct way to reduce the crystallinity of polymers in SPEs. Fillers act as high-modulus linkages in SPEs, which can lower the

glass transition temperature of SPEs and inhibit the crystallization of polymer chains. In addition, fillers increase the cation transfer number due to their Lewis acidity [78]. The high interface impedance is critical problem of SSEs, and effective strategies commonly used to improve interfacial performance include the addition of inorganic or polymer buffer layers to inhibit side reactions and lithium dendrites, the preparation of hybrid electrodes and electrolytes to improve interfacial contact with volume changes during cycling, and the addition of liquid electrolytes or ionic liquids to achieve stable contact at the SSE interface [79]. For example, Han et al. effectively solved the problem of large interfacial impedance between lithium metal anode and garnet electrolyte using atomic layer deposition of ultrathin alumina. The interfacial impedance was significantly reduced from  $1710 \Omega \text{ cm}^2$  to  $1 \Omega \text{ cm}^2$  at room temperature [80]. Zhang et al. added N-methyl-N-propylpiperidinium-bis(fluorosulfonyl) imide ionic liquid between  $\text{Na}_3\text{V}_2(\text{PO}_4)_3$  and NASICON electrolyte as a wetting agent, and  $\text{Na}_3\text{V}_2(\text{PO}_4)_3/\text{Na}$  solid-state batteries have excellent cycling performance and rate capability. After 10,000 cycles at a rate of 10C at room temperature, the specific capacity remained at  $\approx 90 \text{ mAh/g}$  with no capacity decay [81]. In conclusion, the interfacial modification strategies of SSEs should be designed to ensure the full migration of lithium ions at the interface and the stability of the electrochemical reaction process, while different types of SSEs face different interfacial problems, and we present interface problems and typical modification strategies for oxide-based SSEs, sulfide-based SSEs, polymer-based SSEs, respectively.

Oxide-based SSEs have higher hardness and higher interfacial resistance compared with other electrolytes. Therefore, for the interfacial contact problem between oxide SSEs and lithium metal cathodes, researchers mainly use the addition of lithium-friendly interfacial layer to regulate the interface between lithium metal and electrolyte to achieve good contact between electrolyte and lithium metal cathodes [82]. Fu et al. deposited a 20 nm Al coating between the garnet electrolyte and the lithium metal interface, and formed a Li-Al alloy at the interface

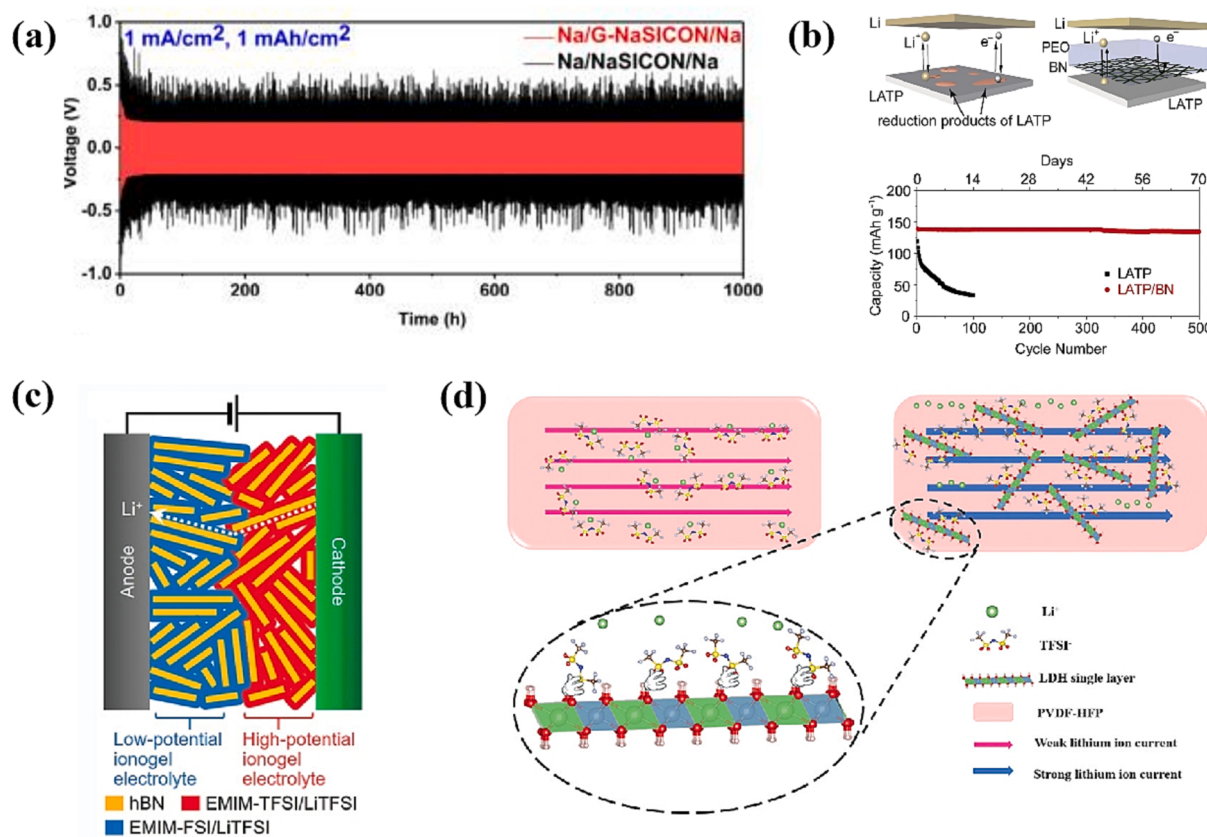


**Fig. 5.** (a) Cyclic stability of Na symmetric battery with current density of  $1 \text{ mA cm}^{-2}$  and capacity of  $1 \text{ mAh cm}^{-2}$  [94]. Copyright 2019, American Chemical Society. (b) Cycle performance of LFP/PEO/LATP/PEO/Li battery with and without boron at  $0.2 \text{ mA cm}^{-2}$  current density [95]. Copyright 2019, Elsevier. (c) Schematic of a solid-state lithium-ion battery using layered heterostructure ionic gel electrolyte with two different ionic liquids and h-BN (hBN) nanosheets [101]. Copyright 2021, John Wiley and Sons. (d) Schematic diagram of lithium-ion conduction mechanism in conventional PVDF-HFP solid polymer system and PVDF-HFP/SLN composite polymer electrolyte (enlarged to show the interaction mechanism between SLN and LiTFSI) [103]. Copyright 2021, John Wiley and Sons.

(Fig. 4a). The formation of Li-Al alloy filled the gap between the garnet electrolyte and the lithium metal, improved the interface contact, and enhanced the transport of lithium-ion. The surface of garnet changed from hydrophobic to hydrophilic. At room temperature ( $20^\circ\text{C}$ ), the interface resistance decreased from  $950 \Omega \text{ cm}^2$  to  $75 \Omega \text{ cm}^2$  [83]. Lou et al. proposed using indium tin oxide (ITO) as the intermediate layer between lithium anode and  $\text{Li}_{6.4}\text{La}_3\text{Zr}_{1.4}\text{Ta}_{0.6}\text{O}_{12}$  (LLZTO) (Fig. 4b). Through the rapid reaction between lithium and ITO intermediate layer, lithium formed an interface composed of lithium oxide,  $\text{Li}_x\text{In}$  and  $\text{Li}_x\text{Sn}$ . The interface resistance of Li/LLZTO dropped sharply from  $1192 \Omega \text{ cm}^2$  to  $32 \Omega \text{ cm}^2$  [84].

Sulfide-based SSEs have a very wide application prospect because of their extremely high ionic conductivity, but there are great problems at the interface with lithium metal electrodes due to their limited electrochemical window. When the lithium metal cathode is in contact with the sulfide electrolyte, interfacial side reactions inevitably occur, leading to uneven current distribution and causing lithium dendrite generation, as well as the problem of lithium dendrite growth [85]. Currently, the solution to the interface problem between sulfide SSE and lithium metal anode is mainly to build the interface layer of electronic insulating ion conduction, and add artificial interface layer at the interface. The main method of constructing the interface layer is to change the interface properties by doping. Han et al. added LiI into  $\text{Li}_2\text{S}-\text{P}_2\text{S}_5$  electrolyte, by adjusting the composition of solid electrolyte interfacial (SEI) on the Li/electrolyte interface, the mobility of  $\text{Li}^+$  was improved, and the deposition of lithium at the interface was promoted, thus effectively inhibiting the formation of lithium dendrites in  $\text{Li}_2\text{S}-\text{P}_2\text{S}_5$  glass. In addition, adding artificial interface layer at the interface could directly avoid the contact between electrolyte and lithium anode, and had a good

inhibition effect on the interface side reaction and lithium dendrite growth [86]. Kato et al. inserted Au film at the interface between lithium metal and  $\text{Li}_2\text{S}-\text{P}_2\text{S}_5$  SSE. Au film was often used as a collector to measure the conductivity of sulfide SSE, and thus Au and sulfide had good compatibility. After the fifth cycle, the utilization rate of lithium metal could still be maintained at about 25% (Fig. 4c), and the morphology of lithium metal was more uniform than that of the battery without Au plating [87].

Polymer-based SSEs are characterized by light mass, good flexibility and good processing properties, but due to their low room temperature ionic conductivity, the performance of SPE is very important in its design, but it can also be used to prepare high-performance batteries by improving the interface performance of electrolyte and lithium anode [88]. Yuan et al. proposed and developed a new design strategy for constructing polyoxometallic polymer electrolyte (PPE) by combining PEO matrix with polyvanadate (LVC). On the one hand, the rigid cluster structure of LVC provided a reinforcing framework for the composite electrolyte, formed a good mechanical solid network, and inhibited the growth of lithium dendrites. On the other hand, LVC could also replace the conduction of  $\text{Li}^+$ , thus improving the transmission capacity of  $\text{Li}^+$ . As shown in Fig. 4d, the lithium symmetrical battery could cycle stably for more than 1300 h at  $0.1 \text{ mA cm}^{-2}$  and  $40^\circ\text{C}$ . It can be seen that adding appropriate fillers into the polymer matrix can effectively inhibit the growth of lithium dendrites and improve the interface stability between the electrolyte and lithium anode [89].

#### 4. Synthesis method of 2D materials for modifying SSE

2D materials have great potential in lithium battery applications.

However, different preparation methods have a certain impact on the properties as well as applications of 2D materials. This paper lists the major methods of preparing 2D materials and presents some studies on the effect of SSE modification with 2D materials prepared by this method.

#### 4.1. Chemical vapor deposition (CVD)

CVD is a method that two or more gaseous substances generate a new solid substance through chemical reaction at high temperature and deposit on the substrate to form a film [90]. After a long period of development, the technology of preparing thin films by the CVD method has now achieved great success in the fields of semiconductors and large-scale integrated circuits. Compared to other preparation processes, CVD has a series of advantages such as controllable parameters, wide applicability, simple equipment, easy control, high product quality, etc [91]. It can realize the growth of large area, continuous, controllable layers, high-quality 2D material films, which is widely used in the preparation of 2D materials and their heterostructures. By changing CVD condition parameters, it can also precisely control the growth of 2D materials and their heterostructures [92].

Graphene is a typical material for CVD growth of 2D materials. Graphene sheet has excellent reversible lithium storage capacity and can be used as electrode material for rechargeable lithium secondary batteries with high magnification and large capacity. Using graphene to manufacture electrochemical energy devices can achieve both high energy density and high power density at high frequencies. Wei et al. used CVD method to directly grow monolayer graphene on Cu foil, and prepared a total thickness of 50  $\mu\text{m}$ . The maximum energy density and maximum power density of this ultra-thin battery reached 10  $\text{wh L}^{-1}$  and 300  $\text{w L}^{-1}$  respectively. It maintained the discharge current density of 100  $\text{uA cm}^{-2}$  in 100 cycles, and the energy retention exceeded 0.02  $\text{mAh cm}^{-2}$ . This is due to the high conductivity of graphene and its huge active area, which can endow lithium-ion conductors and electronic conductors with special properties, thus reducing the size and weight of the battery without sacrificing capacity [93]. Matios et al. also used the unique chemical inertia, mechanical flexibility and structural rigidity of graphene to grow ultra-thin graphene-like network intermediate layer on NASICON ceramic electrolyte through CVD technology to achieve uniform Na plating, reducing the interface resistance by 10 times. Compared with the solid sodium ion battery without graphene as the intermediate layer, the solid sodium ion battery with graphene grown on the NASICON ceramic electrolyte ( $\text{Na}_3\text{Zr}_2\text{Si}_2\text{PO}_{12}$ ) still had a very stable Na plating process after 1000 h cycling at a current density of 1  $\text{mA cm}^{-2}$  and a cycle capacity of 1  $\text{mAh cm}^{-2}$  (Fig. 5a). This is due to the defects on the graphene network providing a channel for  $\text{Na}^+$  migration, realizing the uniform passage of  $\text{Na}^+$  between the SSE and the metal lithium anode, and inhibiting the growth and diffusion of sodium dendrites on the surface of the metal anode [94].

In addition, BN as a 2D material with excellent performance, is chemically and mechanically stable with lithium metal, and can form large-scale, atom-thin and continuous thin films through CVD. BN also has very low electronic conductivity ( $10^{-15} \text{ S cm}^{-1}$ ) and Young's modulus (1.0 TPa), which helps to inhibit the growth of lithium dendrites. More importantly, the BN layer deposited has a mosaic structure and internal defects, which provides a transport channel for lithium-ion. Therefore, the BN layer can provide good protection for SSE without sacrificing the energy density of the battery. Cheng et al. deposited BN film with stable chemical properties and high mechanical strength on LATP pellets by CVD method as the interface protective layer, and added a small amount of PEO or liquid electrolyte to penetrate the interface to enhance the migration of interface ions on the BN layer. When Li/BN interface combined with 1–2  $\mu\text{m}$  PEO polymer electrolyte, the cycle life of Li/Li symmetrical battery exceeded 500 h at 0.3  $\text{mA cm}^{-2}$ . In contrast, the raw LATP failed after 81 h of cycling. The capacity retention rate of LFP/LATP/BN/PEy7O/Li solid-state battery also reached 96.6% after

500 cycles (Fig. 5b) [95]. These results indicated that BN coating grown by CVD was a promising choice as the interface protection layer between lithium metal anode and SSE. Kim et al. synthesized a large area of h-BN film on Cu foil by CVD synthesis transfer technology, and directly grew it on graphene devices. Through parallel capacitance measurement, the dielectric constant of the h-BN film obtained was between 2 ~ 4. The graphene-based transistor with h-BN gate dielectric showed comparable performance before and after the h-BN integration [96].

In addition to graphene and boron nitride, Luo et al. deposited an ultra-thin amorphous Si layer on the SSE by CVD to improve the interface between lithium metal and  $\text{Li}_{6.85}\text{La}_{2.0}\text{Ca}_{0.1}\text{Zr}_{1.75}\text{Nb}_{0.25}\text{O}_{12}$  (LLZ). The ultra-thin (~10 nm) amorphous Si coating could form perfect contact with garnet, and the in-situ reaction between Li and Si generates silicon lithium, which could act as a lithium-ion conductor layer, the wettability of LLZ had changed from ultra-hydrophobic behavior to ultra-lipophilic behavior. Compared with the bare LLZ, the interface impedance of the obtained silicon-coated LLZ symmetrical battery had decreased sharply from  $925 \Omega \text{ cm}^2$  to  $127 \Omega \text{ cm}^2$ , realizing the conversion of the original lithium hydrophobic surface to the lithium hydrophilic surface [97]. Ci et al. reported a heterostructure of defective vanadium selenide ( $\text{VSe}_2$ ) vertical graphene prepared by full CVD to promote the adsorption and conversion of lithium polysulfides in lithium-sulfur batteries,  $\text{VSe}_2\text{-VG@carbon cloth/S}$  electrode had excellent cycle stability at 5.0 C, and the capacity attenuation per cycle was only 0.039% in 800 cycles. The layered  $\text{VSe}_2$  with high specific surface area could provide sufficient surface defects, induced  $\text{VSe}_2$  to convert into  $\text{VS}_2$ , promoted the oxidation and reduction of lithium polysulfide, and improved the cycle stability of lithium sulfur battery [98].

#### 4.2. Exfoliation method

Exfoliation method is one of the main methods for preparing 2D semiconductor materials, which can obtain high-quality, single-layer 2D materials. The mechanism of the exfoliation method is to weaken the interaction between nanosheets [99]. According to its mechanism of action, the exfoliation method can be divided into mechanical exfoliation method, electrochemical exfoliation method, and liquid phase exfoliation method. The interlayer of 2D materials is connected by weak van der Waals forces, making it easy to separate them through external forces. The mechanical peeling method is the simplest and most commonly used method for separating single-layer 2D materials from blocks through external forces [16]. Although the mechanical peeling method can obtain high-quality 2D materials, its cumbersome steps and low efficiency are not conducive to large-scale industrial production; Electrochemical exfoliation method is a method that uses cation intercalation and other methods to apply voltage to the ionic liquid to cause the sample structure to expand, thereby achieving material exfoliation. Electrochemical exfoliation method can overcome the defects caused by mechanical exfoliation method and liquid phase exfoliation method, and obtain defect free crystal structure; Liquid phase exfoliation method refers to placing an object into a solvent that can interact with it, increasing the spacing between layers through the solvent, and then using ultrasonic energy to separate crystals to obtain 2D materials. Although the liquid phase exfoliation method can obtain a large number of single or few layered 2D materials, the sample quality is uncontrollable and poor, making it prone to solvent residues [100].

Hyun et al. prepared h-BN nanosheets from large blocks of h-BN particles by liquid phase exfoliation method, the h-BN nanosheet provided a large surface area to fix the ionic liquid, so as to minimize the mixing at the heterogeneous interface. Fig. 5c demonstrates a schematic diagram of solid-state lithium-ion battery using a hierarchical heterogeneous structured ionic gel electrolyte with two different ionic liquids and h-BN nanosheets. Among them, the hBN nanosheet provided a large surface area to fix the ionic liquid, so as to minimize the mixing at the heterogeneous interface. Compared with the ionic gel electrolyte using mixed ionic liquid, the layered heterogeneous ionic gel electrolyte

extended the electrochemical window, did not produce side effects, and significantly improved the cycle performance [101]. Shen et al. proposed to form a chemically peeled 2D boron nitride nanosheets (BNNSs) protective layer on the surface of PEO based electrolytes. The prepared BNNSs coating formed a sturdy interface layer, improving the chemical and mechanical stability of PEO based electrolytes, inhibiting the growth of lithium dendrites in solid-state lithium metal batteries, and thus improving the performance of solid-state lithium metal batteries. As a result, the all solid-state Li-LFP battery with PEO electrolyte coated with BNNSs provided a specific discharge capacity of  $110 \text{ mA h g}^{-1}$  at 2 C over 200 cycles [102]. Xia et al. prepared single-layer layered-double-hydroxide nanosheets (SLN) reinforced PVDF-HFP composite polymer electrolytes using a liquid exfoliation method, and combined 2D SLN to PVDF-HFP by rational design In matrix, with a small amount of SLN (1 wt%), high ionic conductivity of  $2.2 \times 10^{-4} \text{ S cm}^{-1}$  ( $25^\circ\text{C}$ ), excellent  $\text{Li}^+$  transfer number ( $\approx 0.78$ ) and wide electrochemical window can be obtained ( $\approx 4.9 \text{ V}$ ). Fig. 5d displays a schematic of the lithium-ion conduction mechanism. SLN in the polymer matrix could promote lithium LiTFSI and the immobilization of TFSI<sup>-</sup> anions, thus achieving an enhanced  $\text{Li}^+$  flux in the polymeric matrix. In addition, due to the suitable mechanical strength of the composite polymer electrolyte, the growth of lithium dendrites could also be effectively suppressed. As a consequence, the lithium symmetric battery exhibited an ultra-long-life stable cycle of more than 900 h at  $0.1 \text{ mA cm}^{-2}$  at room temperature. The all-solid-state Li-LFP battery could run stably after 190 cycles at 0.1C and room temperature, and the capacity retention rate was as high as 98.6% [103]. Tang et al. obtained 2D vermiculite sheets (VS) from thermally expanded vermiculite crystals by ion exchange method. 2D VS is used as a filler to enhance SPE, the ionic conductivity of the composite electrolyte at 25, 60 and  $100^\circ\text{C}$  was respectively  $2.9 \times 10^{-5}$ ,  $1.2 \times 10^{-3}$  and  $3.1 \times 10^{-3} \text{ S cm}^{-1}$ , Li-LFP battery with PEO/LiTFSI/10% VS SPE tested at  $60^\circ\text{C}$  displayed much higher capacity (159.9 mAh/g at 0.1 C and 152.0 mAh/g at 0.5 C), attributing to the improvement of the dimensional stability, mechanical strength, ionic conductivity and interfacial stability of the battery by VS fillers, which together helped to inhibit the formation of Li dendrites. The performance of the PEO based SPE modified by VS had been comprehensively improved, including ionic conductivity, mechanical modulus, thermal stability and electrochemical stability, along with reduced flammability and interfacial resistance, for building high-performance solid-state lithium-ion batteries with higher energy and safety [104].

## 5. 2D materials modified SSE

Since the discovery of graphene in 2004 [105], various 2D materials have been gradually applied in battery technology, and 2D materials have played a great role in battery applications by virtue of their unique structure and excellent physicochemical properties [106,107]. On the one hand, the high specific surface area of 2D materials provides a large number of reactive sites, which can provide additional lithium-ion conductive channels and enhance the transmission of lithium-ion [108]. In addition, they offer the advantage of an adjustable bandgap and the ability to tune the physical characteristics to the application [109]. On the other hand, the good spatial structure of 2D materials can bear high stress without structural collapse, thus it can well buffer the volume change of solid-state batteries during charging and discharging, inhibit the formation and growth of dendrites, and reduce the energy barrier of ion migration [110]. These inherent advantages of 2D materials make them become popular materials to meet the challenges of solid-state lithium batteries. According to the type and synthesis of 2D material coatings, they can show different electrochemical behaviors in solid-state lithium batteries [111,112].

First, these materials can provide a range of operating potentials, and the use of 2D materials as electrodes can be used to enhance their electrical conductivity, improve the cycling performance and volumetric capacity of batteries, and increase the availability of active materials

[113]. Encapsulating, mixing, and wrapping the electrode active material with 2D materials to act as a protective layer for the electrode and prevent electrode powdering is also a well-studied method to improve the diffusion path of lithium ions in the electrode active material [114,115]. More interestingly, 2D materials have controllable layer spacing by inserting different polymers or electrolytes, which may improve ion migration and make the electrodes more resistant to cycling-induced volume changes [116].

Second, the use of 2D materials for structural design of electrolytes is also a promising option. Utilizing the unique structure of 2D materials to improve the electrochemical performance of electrolytes has been realized by numerous researchers. 2D materials can reduce the crystallinity of SPEs and increase the room temperature conductivity of SPEs [117]. Meanwhile, the mechanical strength of SPEs is also improved with the application of 2D materials [113]. 2D materials are also used as effective electrolyte heat sinks to reduce the heat generated by the batteries during operation by virtue of their good thermal stability as well as high thermal conductivity [118].

In addition to acting as electrodes and electrolytes, more importantly, 2D materials show unique advantages in modifying SSE. In this regard of inhibiting polysulfide shuttling, Deng et al. have developed a multifunctional interlayer coating consisting of graphitic 2D materials on a separator. They have demonstrated that this 2D crystal structure allows only Li ions to move freely, blocking polysulfide shuttling and effectively improving the ionic conductivity of the electrolyte [119]. In addition, MXene 2D materials with functional groups and defect sites on the surface have been shown to effectively trap polysulfides through chemical and physical adsorption [120]. In terms of promoting uniform deposition/stripping of lithium and improving the electrode/electrolyte interfacial resistance, the 2D materials can effectively inhibit the occurrence of side reactions and improve the interfacial stability. Chu et al. mitigated the volumetric expansion of lithium anodes during long-term cycling by mixing customized 2D metal-organic framework particles with a typical carbonate electrolyte, resulting in an ultrastable plating/stripping cycle of lithium of at least 1400 h [121]. Utilizing 2D materials as protective coatings for SSEs is one of the techniques to improve the electrochemical performance of SSEs, and their excellent mechanical properties can inhibit the growth of lithium dendrites and prolong the performance and lifetime of the batteries. Liu et al. succeeded in designing and fabricating a new 2D hierarchical structure by grafting trichromatic poly(lithium styrenesulfonate) (PSSLi) chains onto both sides of graphene oxide (GO) sheets, and through evaporation induction further constructed GO-g-PSSLi ultrathin films. The graphene oxide skeleton inside the film has a rigid 2D extended aromatic structure, which can play a shielding role and effectively prevent the possible lithium dendrites from penetrating into the diaphragm at high current densities [122]. Different 2D materials have different effects on the interfacial modification of SSEs, so the effects of different 2D materials on the interfacial modification of SSEs are categorized and elucidated below.

### 5.1. Molybdenum disulfide ( $\text{MoS}_2$ )

Recently, the application of  $\text{MoS}_2$  as an interface protection layer in solid-state batteries has achieved great success and is expected to become a candidate material for interface protection layer [123,124].  $\text{MoS}_2$  as a 2D transition metal dihalide compound, which has a larger interlayer distance of 0.62 nm (about twice that of graphene) [125,126]. The layers are connected with each other through a weak van der Waals force, so that  $\text{Li}^+$  transmission is not hindered and can be loosely adsorbed on  $\text{MoS}_2$  defects, which promotes the faster diffusion of lithium-ion [127]. In addition,  $\text{MoS}_2$  can inhibit the dissolution of polysulfides to reduce the shuttle effect in lithium sulfur batteries. Compared with other coating materials (such as carbon,  $\text{Al}_2\text{O}_3$  and polymers),  $\text{MoS}_2$  shows higher ionic conductivity and lower electronic conductivity, which is of great significance for the development of high-

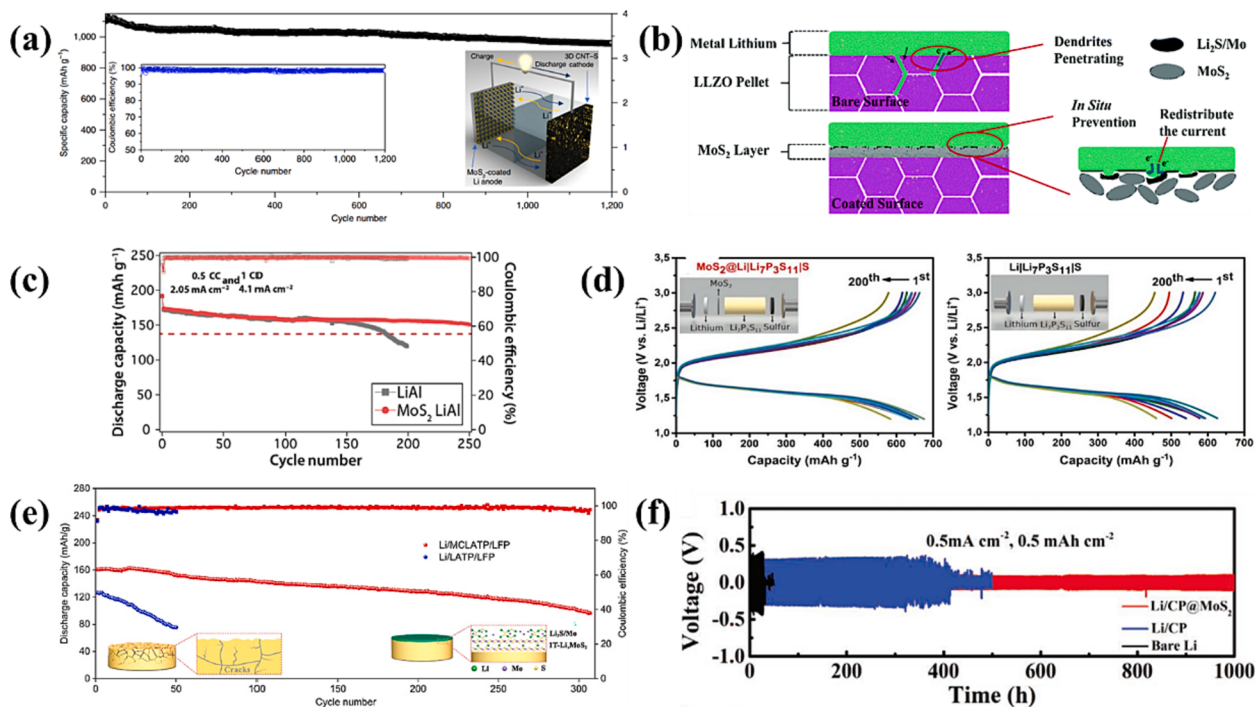


**Fig. 6.** (a) Long term cycle performance of lithium battery with MoS<sub>2</sub> coated lithium as anode [19]. Copyright 2018, Springer Nature. (b) Schematic illustration of the in situ MoS<sub>2</sub> protection mechanism [129]. Copyright 2019, Royal Society of Chemistry. (c) Cycle curves based on LiAl/NCM811 and MoS<sub>2</sub> LiAl/NCM811 full cells at 0.5 C charge capacity and 1 C discharge capacity with a voltage window of 2.7 to 4.3 V [130]. Copyright 2019, Authors, licensed under a Creative Commons Attribution NonCommercial License 4.0 (CC BY-NC). (d) Galvanostatic charge–discharge analysis of all solid-state MoS<sub>2</sub>@Li/Li<sub>7</sub>P<sub>3</sub>S<sub>11</sub>/S and Li/Li<sub>7</sub>P<sub>3</sub>S<sub>11</sub>/S cells [131]. Copyright 2020, John Wiley and Sons. (e) Long-term cycling test of Li/LATP/LFP and Li/MCLATP/LFP cells at 1 C [132]. Copyright 2022, Elsevier. (f) Cycling performance of the Li-Li symmetrical cells assembled with bare Li, Li/CP, and Li/CP@MoS<sub>2</sub> anodes [134]. Copyright 2020, John Wiley and Sons.

performance solid-state batteries [128].

Similar to graphene, MoS<sub>2</sub> is composed of hexagonal lattice layer structure formed by covalent bonding of Mo-S-Mo units, whose unique structure and phase transition characteristics resolve the problems of high impedance and poor contact at the interface. Cha et al. used 2D MoS<sub>2</sub> as the protective layer of the lithium metal anode in the liquid-based lithium-sulfur battery. The Li-S full battery with MoS<sub>2</sub> coated lithium as the anode obtained a specific energy density of about 589 Wh kg<sup>-1</sup> and a coulomb efficiency of about 98% at 0.5 C. After 1200 cycles, it also retained 84% of the high capacity (Fig. 6a), which highlighted the key role of MoS<sub>2</sub> as the interface protective layer in the lithium-sulfur battery. The MoS<sub>2</sub> protective layer could directly insert Li atoms into its atomic layer structure, reduce the interface resistance, promote the migration of Li<sup>+</sup> at the interface, realize the stable deposition/dissolution of lithium, and prevent the formation of lithium dendrites [19]. Fu et al. also used this feature to coat MoS<sub>2</sub> coating on bare Li<sub>6.5</sub>La<sub>3</sub>Zr<sub>1.5</sub>Ta<sub>0.5</sub>O<sub>12</sub> (LLZO) particles. MoS<sub>2</sub> converted at the interface and formed a dynamic stable intermediate layer in situ, effectively inhibiting the local tip electric field effect and the growth of lithium dendrites, reducing the interface resistance to only 14 Ω cm<sup>2</sup>, and increasing the critical current density of the battery from 0.7 mA cm<sup>-2</sup> to 2.2 mA cm<sup>-2</sup>, Fig. 6b presents a schematic of the protection mechanism of in situ MoS<sub>2</sub>. This is because the in-situ reaction of MoS<sub>2</sub> generates a Li<sub>2</sub>S/Mo intermediate layer, which reduces the interface resistance between lithium anode and SSE, and also promotes the uniform deposition/dissolution of lithium and inhibits the formation of dendrites [129]. Kim et al. used a lithium-aluminum (LiAl) anode composed of Li and Li<sub>9</sub>Al<sub>4</sub> intermetallic compounds and a well-designed Langmuir-Blodgett artificial SEI (LBSEI) composed of MoS<sub>2</sub> as the electrolyte, highly loaded LiNi<sub>0.8</sub>Coo<sub>0.1</sub>Mn<sub>0.1</sub>O<sub>2</sub> (NCM811) as cathode. Full battery could be charged at 0.5 C and discharged at 1 C for up to 250 cycles with over 80% capacity retention (Fig. 6c). However, the whole battery of LiAl anode failed after 180 cycles, suggesting that the use of MoS<sub>2</sub> protective layer not only

improved the migration of lithium-ion at the interface, but also promoted the compact deposition of lithium-ion on the large surface of the anode and increased the cycle life of the whole battery [130].

It is feasible to use the layered structure of MoS<sub>2</sub> hexagonal lattice as the intermediate layer, Kizilaslan et al. used artificial 2H-MoS<sub>2</sub> layer to modify the surface of metal lithium anode to prevent the contact of highly active lithium with SSE, by stabilizing the electrode/electrolyte interface, the initial discharge capacity was 675.8 mAh/g and the final discharge capacity was 584.1 mAh/g in MoS<sub>2</sub>@Li/Li<sub>7</sub>P<sub>3</sub>S<sub>11</sub>/S when the current density was 0.4 mA cm<sup>-2</sup>. After 200 cycles, the discharge capacity of the battery with 2H-MoS<sub>2</sub> modified lithium anode decreased by 13.58%, while that of the bare lithium anode battery decreased by 27.3% (Fig. 6d), this is because MoS<sub>2</sub> as an artificial SSE film effectively prevented the degradation of SSE and the corrosion of lithium anode, thus reducing the total impedance of the battery [131]. Huang et al. proposed to use MoS<sub>2</sub> as an artificial SSE interface to modify NASICON-type electrolyte. The MoS<sub>2</sub> coating was evenly coated on the surface of LATP, which significantly reduced the charge transfer resistance and improved the ion transfer performance of the interface. Through the interface modification of MoS<sub>2</sub>, the symmetrical battery showed slight polarization. MoS<sub>2</sub> coated LATP (MCLATP) as electrolyte and LFP as anode, the Li/MCLATP/LFP battery showed excellent cycle performance in 300 cycles at 1 C. However, after 50 cycles, the capacity of Li/LATP/LFP battery was only 75.3 mAh/g, the corresponding capacity retention rate was about 60% (Fig. 6e) [132]. This was due to the modification of MoS<sub>2</sub>, the battery exhibited smaller charge transfer resistance and polarization, and the conversion layer composed of Li<sub>2</sub>S and Mo metal was formed in situ during the cycle, which not only regulated the interface mass transfer and improved the charge transfer dynamics, but also inhibited the decomposition of LATP. In addition, the enhancement of the conductivity of the MoS<sub>2</sub> interlayer eliminated the priority site of Li dendrite nucleation, and realized the high-performance Li-S battery. In view of the protective characteristics of MoS<sub>2</sub> coating, Cha et al.

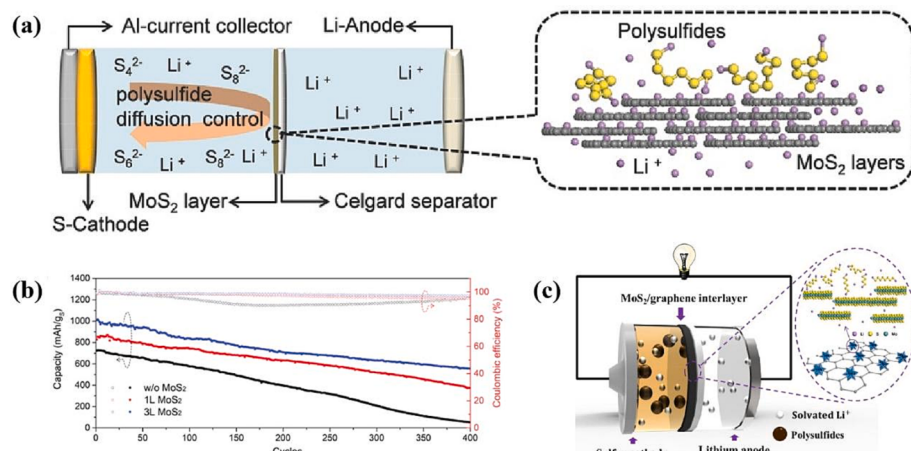


**Fig. 7.** (a) Schematic cell configuration of Li-S batteries using MoS<sub>2</sub>/Celgard separator [136]. Copyright 2017, John Wiley and Sons. (b) Long term cycle performance of MoS<sub>2</sub> diaphragms of different quantities at 0.5 C [137]. Copyright 2019, American Chemical Society. (c) Schematic of the electrode configuration for the designed Li-S batteries with an MoS<sub>2</sub>/graphene interlayer [138]. Copyright 2017, Elsevier.

introduced MoS<sub>2</sub> protective coating on the lithium metal anode, and used NCM811 as the cathode and traditional carbonate electrolyte to assemble the coin battery. The results showed that the bare lithium battery showed serious capacity decline after the 20th cycle, while the lithium anode with MoS<sub>2</sub> coating showed a serious capacity decline when the cathode load was 4.2 mAh cm<sup>-2</sup>, and the E/C ratio was 3 g Ah<sup>-1</sup>. In addition, the battery showed up to 170 stable cycles with a capacity of about 80%, which was due to the introduction of MoS<sub>2</sub> coating effectively inhibiting the growth of lithium dendrites and the loss of metal lithium caused by interface reaction, thus extending the cycle life of lithium metal battery under the condition of poor electrolyte [133]. During electroplating, Mo and Li show strong affinity, which can guide Li to nucleate rapidly and selectively deposit on Mo surface with large specific surface area, thus reducing local current density. Yang et al. used MoS<sub>2</sub> as a Li pre-nucleating agent to promote the uniform deposition of lithium. The MoS<sub>2</sub> prenucleator is grown on a carbon paper (CP), which acts as an interlayer between the SPE and Li anode (labeled as CP@MoS<sub>2</sub>). The lithium-ion symmetrical battery in the pre-nucleating of MoS<sub>2</sub> showed excellent electrochemical performance, with a cycle life of up to 1000 h and 780 h at 1 mA cm<sup>-2</sup> and 0.5 mA cm<sup>-2</sup> current densities (Fig. 6f). The Li-LFP all-solid-state lithium battery showed a high capacity retention rate of 78% and an ultra-long cycle life of 3000 times at 1 mA cm<sup>-2</sup> current densities. At the initial stage of lithium plating, MoS<sub>2</sub> was reduced to eukaryotic body (Mo) and Li<sub>2</sub>S, Mo

had high affinity with Li, which lead to homogeneous nucleation and selective deposition of Li [134].

In addition to being used as the interface protection layer, MoS<sub>2</sub> can also be used as the interlayer material of lithium battery separator to reduce the shuttle effect of polysulfide. Li-S batteries form lithium polysulfides (LiPSs) during electrochemical reactions. LiPSs is soluble in the electrolyte and is free to diffuse to the anode and irreversibly react with lithium metal. This process, known as the shuttle effect, leads to the loss of active material and rapid decay of battery capacity [135]. Due to the 2D flexible nature of MoS<sub>2</sub>, a flexible MoS<sub>2</sub>/Celgard composite separator can be easily deposited on a conventional Celgard separator by simple filtration of a thin layer of MoS<sub>2</sub>. When used in Li-S batteries, the barrier can block the diffusion of polysulfides, which significantly inhibits polysulfides shuttling, resulting in a high Coulombic efficiency (Fig. 7a). Ghazi et al. used MoS<sub>2</sub>/Celgard composite membrane as polysulfide barrier in Li-S battery. After 600 cycles, the coulomb efficiency remained above 99.5%, and the actual capacity was 401 mAh/g, which corresponds to only 0.083% capacity attenuation per week. Due to the high density of lithium-ion on the surface of MoS<sub>2</sub>, the composite membrane had high lithium conductivity, rapid lithium-ion diffusion rate, and convenient lithium migration. When used in Li-S battery, The composite diaphragm could effectively inhibit the shuttle effect of polysulfides, thus obtaining high and long cycle stability [136]. Similarly, Yu et al. used the self-developed MoS<sub>2</sub> ultrathin layer in Li-S batteries.

**Table 2**  
Electrochemical performance of batteries with MoS<sub>2</sub>-modified materials.

Anode/Cathode	Coating layer	Electrolyte	Mechanism	Performance	Capacity Retention Rate/%	Ref
Li/3D carbon nanotube-sulfur	MoS <sub>2</sub>	LiTFSI/LiNO <sub>3</sub>	As a protective layer for Li-metal anodes	over 1200 cycles at 0.5C	84	[19]
Li/Li	MoS <sub>2</sub>	Li <sub>6.5</sub> La <sub>3</sub> Zr <sub>1.5</sub> Ta <sub>0.5</sub> O <sub>12</sub>	Build conversion reaction Li <sub>2</sub> S/Mo layer	over 150 h at 0.2 mA cm <sup>-2</sup>	–	[129]
LiAl/NCM811	Langmuir Blodgett MoS <sub>2</sub>	LBASEI	As artificial SEI to protect LiAl anode	over 250 cycles at 0.5 CC and 1CD	80	[130]
Li/S	2H MoS <sub>2</sub>	Li <sub>2</sub> P <sub>3</sub> S <sub>11</sub>	Stable electrode electrolyte interface	200 cycles at 0.4 mA cm <sup>-2</sup>	86	[131]
Li/LFP	MoS <sub>2</sub>	LATP	Interfacial modification	over 300 cycles at 1 C	60	[132]
Li/NCM811	MoS <sub>2</sub>	Carbonate	Preventing dendrite growths and electrolyte dry-out	3000 cycles at 1 mA cm <sup>-2</sup>	78	[133]
Li/LFP	MoS <sub>2</sub>	SPE	Promoting Li uniform nucleation and selective deposition	3000 cycles at 1C	78	[134]
Li/S	MoS <sub>2</sub>	Celgard	Depressing PSs shuttle	600 cycles at 0.5 C	46	[136]
Li/carbon nanofiber + Li <sub>2</sub> S <sub>8</sub>	10~40 nm MoS <sub>2</sub>	Celgard separator	Mitigating the shuttle effect in Li-S batteries	400 cycles at 0.5 C	55	[137]
Li/S	composited 2D MoS <sub>2</sub> and graphene	Lithium polysulfides	Preventing the shuttle of polysulfide	200 cycles at 1 A/g	74	[138]

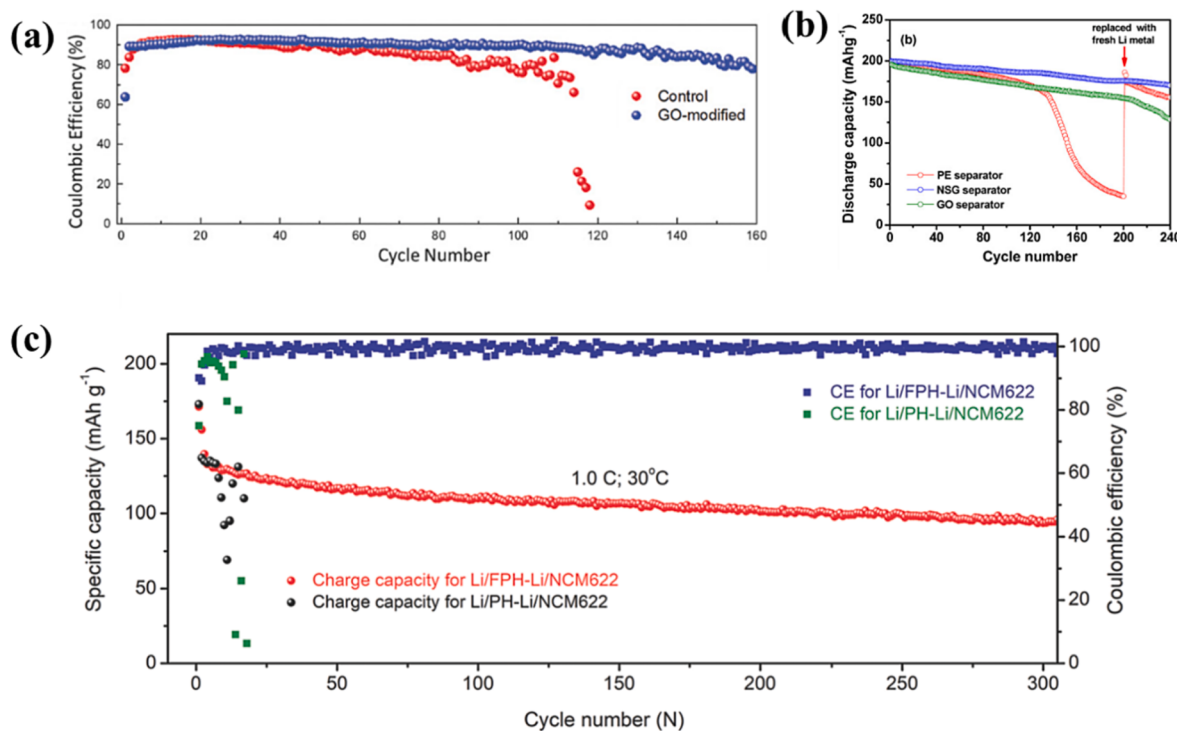


**Fig. 8.** (a) Coulomb efficiency of diaphragm free and GO modified Li-Cu semi battery [142]. Copyright 2018, John Wiley and Sons. (b) Discharge capacity of Li/LiNi<sub>0.8</sub>Co<sub>0.15</sub>Al<sub>0.05</sub>O<sub>2</sub> battery assembled with different diaphragms changes with the number of cycles [18]. Copyright 2015, American Chemical Society. (c) Cycling performance of Li/FPH-Li/NCM622 and Li/PH-Li/NCM622 cells at 1 C [146]. Copyright 2022, John Wiley and Sons.

The thin layer could be easily peeled off to form a chemically stable thin sheet with a large area to thickness ratio (aspect ratio). The results indicated that the battery coated with enough MoS<sub>2</sub> diaphragm displayed the minimum capacity attenuation at the rate of 0.5 C (Fig. 7b), which showed that the 2D structure of MoS<sub>2</sub> as the diaphragm material effectively slowed down the diffusion of LiPS, the chemical performance and cycle efficiency of Li-S battery were improved [137]. In addition, MoS<sub>2</sub> can also be designed with carbon materials to stabilize lithium batteries. Guo et al. developed a dual-functional MoS<sub>2</sub>/graphene interlayer, in which graphene provided a conductive network to adapt to the electronic transfer of polysulfides, and MoS<sub>2</sub> acted as a chemical barrier to prevent the shuttle of polysulfides (Fig. 7c). When the current density was 0.5, 1.0, 2.0 and 3.0 A/g, the specific capacity of the whole battery with MoS<sub>2</sub>/graphene interlayer was 850, 770, 701 and 600 mAh/g respectively. In addition, even after 200 cycles, the battery still maintained the reversible capacity of 718 mAh/g, which showed that the MoS<sub>2</sub>/graphene interlayer effectively lowered the shuttle effect, decreased the polarization of the sulfur cathode, and the Li-S battery exhibited excellent cycle rate performance [138]. We summarize the electrochemical performance of SSE modified by MoS<sub>2</sub> in recent years, as shown in Table 2.

## 5.2. Graphene and its derivatives

Graphene has high conductivity ( $\approx 10^6$  S cm<sup>-1</sup>), high specific surface area ( $\approx 2630$  m<sup>2</sup> g<sup>-1</sup>), and high lithium capacity, as well as excellent electrochemical performance and layered structure, making it one of the most promising materials for all solid-state lithium batteries [139]. Li et al. added an inorganic composite interlayer (ICI) between the cathode and LLZTO electrolyte. The ICI was formed by the in-situ conversion of fluorosilane. Graphene was used to improve the interface contact between LiF and garnet electrolyte. LiF was used to enhance the transmission of lithium-ion on the cathode side. The interface resistance of the Li/LLZTO/ICI/LFP solid-state lithium battery assembled from this interlayer was about 5 times lower than that without this interlayer, the

battery was successfully cycled at 0.05 C and 60 °C, and showed 90% capacity retention after 60 cycles, indicating that LiF-graphene can improve the interface contact between cathode and garnet electrolyte [140].

As an oxidation derivative of graphene, GO has a similar structure to graphene and is one of the most common 2D materials used as diaphragm coating so far. Due to its easy synthesis, high mechanical strength (Young's modulus close to 300 GPa), good flexibility (bending modulus close to 1 kT) and electrical insulation, it is widely used in solid lithium batteries [141]. Foroozan et al. reported a kind of graphene oxide nanosheet (GO) coating used for glass fiber diaphragm. When the coating was not modified, the battery capacity decreased to below 80% after 80 cycles, and reached below 20% after 115 cycles. However, the capacity of the GO-modified battery only decreased to 83% after 160 cycles. Compared with the best control sample of 80 cycles, the recyclability of Li metal was increased by about 2 times (Fig. 8a), this was due to the structure of GO coating promoting the diffusion of lithium-ion and regulating the uniform deposition of lithium [142]. Jia et al. added GO as nano-filler to LiClO<sub>4</sub>-poly-acrylonitrile (PAN) type SPE with different weight percentage, and the ionic conductivity of composite SPE containing 1.0 wt% GO reached  $2.6 \times 10^{-4}$  S cm<sup>-1</sup> at room temperature, which was one order of magnitude higher than the bare SPE ( $2.2 \times 10^{-5}$  S cm<sup>-1</sup> at 30 °C), in addition, LFP battery with 1.0 wt% GO-SPE as electrolyte exhibited a satisfactory average discharge capacity of 166 mAh/g at 0.2 C, which was superior to the performance of GO-free battery (136 mAh/g) [143]. This was because GO could help the dissociation of LiClO<sub>4</sub> in PAN matrix, alleviating the polarity of carbon–nitrogen bonds and making the polymer more flexible. Zhuang et al. studied the electrochemical and chemical interface reaction mechanism between LiNi<sub>0.5</sub>Co<sub>0.2</sub>Mn<sub>0.3</sub>O<sub>2</sub> (NMC532) and poly (propylene carbonate) solid polymer electrolyte (PPC-SPE). By coating GO on LiNi<sub>0.5</sub>Co<sub>0.2</sub>Mn<sub>0.3</sub>O<sub>2</sub> particles, compared with the original cathode, the coating sample showed higher initial capacity, better cycle stability and lower interface resistance, and the capacity retention rate after 300 cycles at 0.3 C was 69.2%, the interface resistance after 180 cycles was

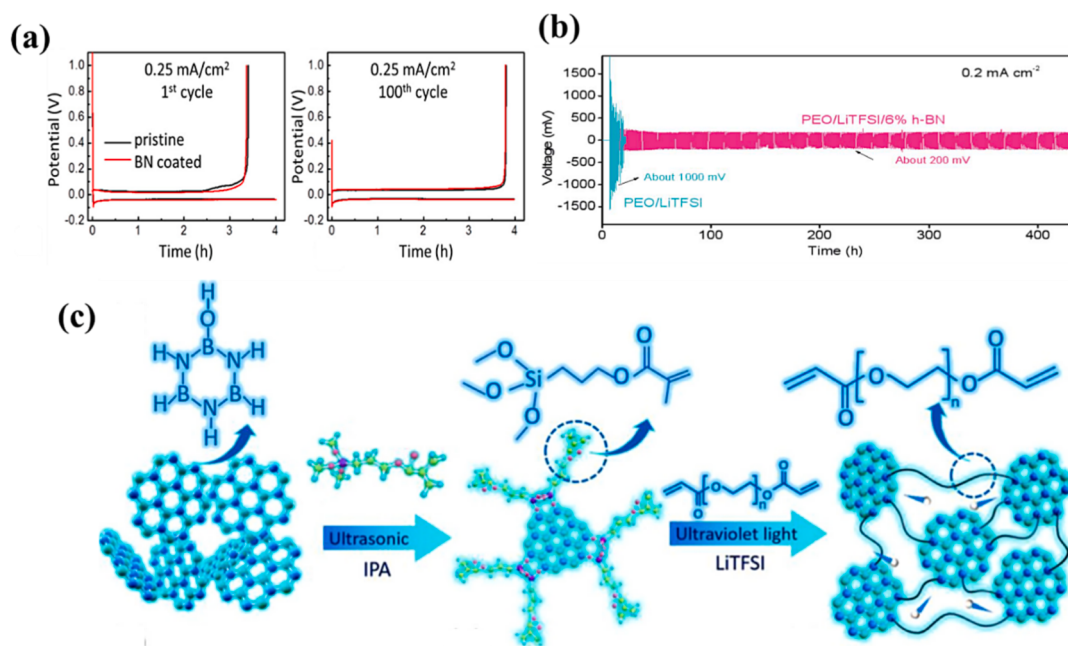


**Fig. 9.** (a) Electrochemical performance of Li-Cu battery with original diaphragm (black) and BN coated diaphragm (red) at current density of  $0.5 \text{ mA cm}^{-2}$  and  $1.0 \text{ mA cm}^{-2}$  [118]. Copyright 2015, American Chemical Society. (b) Long-term cycling performance of the Li metal battery with the PEO/LiTFSI/6% h-BN composite electrolyte and the PEO/LiTFSI SPE at  $60^\circ\text{C}$  [151]. Copyright 2020, Royal Society of Chemistry. (c) Schematic diagram of the synthesis process of BNP [153]. Copyright 2021, Elsevier. (For interpretation of the references to colour in this figure legend, the reader is referred to the web version of this article.)

$25 \Omega$ , which was because the graphene layer promoted the interface charge transfer process and slowed down the cathode/electrolyte interface side reaction [144]. Gomari et al. prepared a nanocomposite SPE of polyethylene glycol grafted graphene (FGnP), PEO and lithium perchlorate ( $\text{LiClO}_4$ ). The ionic conductivity of SPE/FGnP nanocomposite electrolyte reached the maximum of  $2.53 \times 10^{-5} \text{ S cm}^{-1}$  at room temperature (about 19 times higher than that of pure SPE). At the same time, after adding FGnP, the interaction between FGnP and PEO led to strong adhesion between filler and matrix, the mechanical properties (including tensile strength, toughness and elongation at break) of the nanocomposite film were also significantly improved, which showed that the addition of functional graphene also improved the ionic conductivity and mechanical properties of the SPE used for flexible devices [145]. Shin et al. also deposited nitrogen-sulfur co-doped graphene (NSG) nanosheet coating on the polyethylene (PE) separator through vacuum infiltration, effectively inhibiting the growth of dendrites. The results displayed that the electrochemical performance of the lithium metal battery composed of  $\text{LiNi}_{0.8}\text{Co}_{0.15}\text{Al}_{0.05}\text{O}_2$  cathode and NSG coated separator was significantly better than that of the battery without PE separator. Compared with the bare PE separator, the NSG coated PE separator could reduce the charge transfer resistance of lithium-ion by 6 times after 200 cycles (Fig. 8b), which showed that the skeleton structure of NSG was conducive to lithium-ion migration and could stabilize the surface of lithium electrode, suppress dendrite formation and improve cycle stability of lithium metal battery [18]. Zhai et al. reported that 2D fluorinated graphene-reinforced PVDF-HFP-LiTFSI (FPH-Li) SPE to build an artificial interface layer. The 2D fluorinated graphene was evenly distributed on the surface of the electrolyte, effectively improving the mechanical properties of the battery, preventing the side reaction of lithium metal anode and electrolyte, improving the conductivity of  $\text{Li}^+$  and promoting the uniform deposition of Li, and thus high Li ionic conductivity ( $1.32 \times 10^{-4} \text{ S cm}^{-1}$  at  $30^\circ\text{C}$ ) is obtained at room temperature. The Li/FPH-Li/NCM622 full battery modified by 2D fluorinated graphene could operate stably for more than 300 cycles at 1 C, with a capacity retention rate of about 81.5% and an average coulomb efficiency of 99.5%. However, the capacity of Li/PVDF-HFP-LiTFSI/NCM622 (Li/PH-Li/NCM622) battery decayed rapidly, and the battery

failed only after 15 cycles (Fig. 8c). The Li/FPH-Li/Li pair modified by 2D fluorinated graphene still kept stable cycle without short circuit even at  $1.0 \text{ mA cm}^{-2}$ . In contrast, when the current density increased to  $0.1 \text{ mA cm}^{-2}$ , the Li/PH-Li/Li symmetrical battery would have a short circuit [146].

### 5.3. Boron nitride (BN)

Similar to graphene, BN is a layered structure with good electronic insulation and chemical/electrochemical stability. Due to the layered structure of BN, it can isolate the direct contact between the electrolyte and the electrode, thus inhibiting the reaction and improving the interface stability [147]. Xu et al. used this property of BN to doped BN into  $\text{Li}_7\text{P}_3\text{S}_{11}$  (LPS) SSE. BN nanoflakes could partially isolate  $\text{Li}_7\text{P}_3\text{S}_{11}$  SSE and lithium metal. For Li-S batteries with LPS, LPS-1% BN, LPS-2% BN and LPS-3% BN SSE, the initial charging capacity of all solid-state Li-S batteries was 400.6, 482.5, 646.5, 495.2 mAh/g, the initial coulomb efficiency was 48.1%, 59.4%, 80.4% and 62.7%, respectively. The low initial coulomb efficiency of LPS SSE Li-S battery may be caused by the reaction between LPS and lithium anode. BN nanoparticles coated on LPS particles can effectively isolate the direct contact between LPS and lithium metal, thus improving the interface compatibility between electrode and electrolyte. With the increase of BN doping content, the ionic conductivity of SSE will decrease, which shows worse performance. In short, using BN-doped LPS as a SSE, the all-solid-state Li-S battery demonstrated enhanced electrochemical performance, better cycle stability and higher coulomb efficiency [148].

2D BN can also be used as an additive in electrolyte to bring high ionic conductivity, improved mechanical strength and close interface contact to lithium battery. Zhang et al. added 1% BN to the poly (vinylidene fluoride-co-hexafluoropropylene)/LiTFSI (PVDF-HFP/LiTFSI) mixed electrolyte membrane, and the electrolyte modified by BN showed  $1.82 \times 10^{-3} \text{ S cm}^{-1}$  at room temperature high ionic conductivity. The indentation test displayed that the hardness (4.99 MPa) and Young's modulus (0.133 GPa) of the electrolyte were enhanced, which effectively inhibited the growth of lithium dendrites during the repeated stripping and electroplating of lithium. As a result, battery composed of

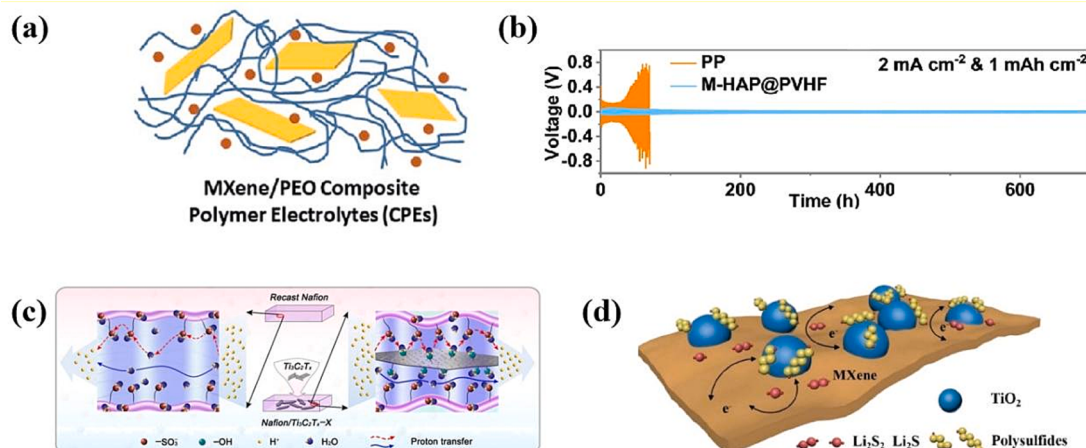


**Fig. 10.** (a) Schematic diagram of MXene/PEO CPEs [159]. Copyright 2019, Royal Society of Chemistry. (b) Cycling behaviors of Li/Li symmetric cells with the PP, M-HAP@PVHF separators ( $2 \text{ mA cm}^{-2}$  &  $1 \text{ mAh cm}^{-2}$ ) [162]. Copyright 2022, Elsevier. (c) Schematic illustration of proton transfer through recast Nafion and Nafion/Ti<sub>3</sub>C<sub>2</sub>T<sub>x</sub>-X [163]. Copyright 2016, American Chemical Society. (d) Schematic illustration of LiPSs trapping and conversion process on the TiO<sub>2</sub>-Ti<sub>3</sub>C<sub>2</sub>T<sub>x</sub> heterostructures [167]. Copyright 2019, John Wiley and Sons.

lithium metal anode and LFP catalyst using the as-fabricated 1% BN enhanced polymer/salt hybrid electrolyte exhibited improved cycling performance (116 mAh/g after 50 cycles at 0.2 C) with high Coulombic efficiency (over 98%). In addition, BN could also improve the thermal performance of the electrolyte [149].

Due to its excellent chemical properties, BN can also be used to modify SSE. In order to inhibit the formation and growth of lithium dendrites, Luo et al. developed a 2D h-BN nanosheet (BNNs) coated thermal barrier, which is used as a barrier in traditional organic carbonate based electrolyte. The results displayed that the current density was  $0.5 \text{ mA cm}^{-2}$  and  $1.0 \text{ mA cm}^{-2}$ , the coulomb efficiency was stable at 92% and 88% after 100 cycles (Fig. 9a). The improvement of coulomb efficiency and reliability of lithium metal anode was due to the more uniform heat distribution of thermal conductivity BN coating and the smaller surface area of initial lithium deposition. BNN coating promoted the uniform stripping of Li<sup>+</sup>, reduced the formation of lithium dendrites, and improved the cycling performance of the battery, especially at high current density [118]. In order to stabilize lithium metal anode, Yan et al. grew atomic crystal layers of h-BN and graphene on copper metal collector by chemical vapor deposition, forming a 2D layer-Li-Cu interlayer structure. In the process of electrochemical deposition, Li<sup>+</sup> could penetrate the point defects and line defects of the 2D layer and promote the uniform deposition of lithium. At the same time, the strong intra-layer bonding and ultra-thin thickness of the 2D layer provided good interface protection for lithium metal and inhibited the growth of dendrites. In organic carbonate electrolyte, when the current density and area capacity reached  $2.0 \text{ mA cm}^{-2}$  and  $5.0 \text{ mAh cm}^{-2}$ , respectively, it showed more than 50 stable cycles and 97% coulomb efficiency, which was significantly better than that of the unprotected electrode in the same electrolyte [150]. Li et al. restricted the movement of anions by adding h-BN to the PEO-based SPE to inhibit the growth of lithium dendrites. As a result, the diffusion of TFSI<sup>-</sup> showed a more significant decline in the presence of h-BN. This indicated that the presence of BN inhibited the movement of anions and enhanced the selectivity of Li<sup>+</sup> transport. PEO/LiTFSI/h-BN composite electrolyte demonstrated higher lithium-ion conductivity than PEO/LiTFSI system, but the anion diffusion rate was lower. Therefore, the all-solid polymer lithium metal/LFP battery with PEO/LiTFSI/h-BN composite electrolyte displayed high initial capacity (143.3 mAh/g) and capacity retention rate (93%) after 140 cycles (Fig. 9b). At the same time, Li/CPE/Li could be stabilized for 430 h at  $0.2 \text{ mA cm}^{-2}$  due to stable interface contact [151]. Yin et al. introduced 2D BN into the mixed PEO-PVDF LiTFSI polymer to form a new solid composite electrolyte. At a temperature of more than 60 °C,

the ionic conductivity of BN-PEO-PVDF sample was about  $10^{-4} \text{ S cm}^{-1}$  higher than that of PEO-PVDF sample ( $\approx 10^{-5} \text{ S cm}^{-1}$ ). At 70 °C and  $0.1 \text{ mA cm}^{-2}$ , the overvoltage of lithium symmetrical battery with BN-PEO-PVDF remained low ( $\approx 40 \text{ mV}$ ) for more than 200 h. However, the overvoltage of PEO-PVDF lithium symmetrical battery gradually increased to about 100 mV, and there was a sign of short circuit only after 55 h, which showed that BN nanosheet not only improved the ionic and mechanical properties of the electrolyte, but also promoted more stable and effective lithium metal stripping and deposition [152]. An et al. designed an interpenetrating polymer network electrolyte BNNs-MPS-PEGDA (BNP) by chemical graft coupling, as shown in Fig. 9c, in which 2D boron nitride nanosheets (BNN) and polyethylene glycol diacrylate (PEGDA) were coupled by silane coupling agent (MPS). The mechanical strength of the SPE was considerably enhanced by the graft-coupling strategy, and the Li-Li symmetric cell exhibited good stability in the  $>2000 \text{ h}$  cycle test. In addition, the full cell using LFP as the cathode was able to exhibit excellent cycling performance with 80% capacity retention over 600 cycles due to the stable electrochemical window of BNP ( $\approx 5.5 \text{ V}$  vs Li/Li<sup>+</sup>), and the full cell using NCM811 had 87.5% capacity retention after 150 cycles at room temperature [153].

#### 5.4. MXene

MXene is a 2D material composed of transition metal carbides, nitrides, or carbon-nitrides, which can be represented by  $M_{n+1}X_nT_x$ , where M denotes a transition metal, X denotes carbon or nitrogen, and  $T_x$  denotes a surface functional group [154]. Since the discovery of Ti<sub>3</sub>C<sub>2</sub>T<sub>x</sub> by Gogotsi et al. in 2011, more than 30 new MXenes have now been synthesized, and MXenes will continue to be a hotspot for 2D materials research in the future as well [155]. MXene, as a new type of 2D layered structural material, possesses excellent electronic conductivity, rich surface chemistry and a variety of tunable chemical, electrical, mechanical and optical properties, it has been widely used in high-end fields such as energy storage, catalysis, sensing and medicine [156,157].

Due to the presence of multifunctional functional groups on the surface, MXene can be well dispersed in aqueous solutions and some organic solvents, and for CPE, this hydrophilic surface enhances the interactions between MXene and polymer chains, which reduces the crystallinity of PEO and improves the ionic conductivity [158]. For this reason, Pan et al. prepared MXene-based CPE by homogeneously dispersing a small amount of Ti<sub>3</sub>C<sub>2</sub>T<sub>x</sub> into a PEO/LiTFSI complex (PEO<sub>20</sub>-LiTFSI) using an aqueous solution blending method (Fig. 10a). MXenes showed higher efficiency in ionic conductivity enhancement

**Table 3**

Electrochemical performance of batteries with 2D materials-modified SSEs.

Anode/Cathode	2D materials	SSEs	Performance	Capacity	Retention Rate/%	Ref
Li/LFP	LiF/graphene	LLZTO	60 cycles at 0.05 C and 60 °C	90	[140]	
Li/Cu	GOn	LiPF <sub>6</sub>	160 cycles at 1 mA cm <sup>-2</sup>	83	[142]	
Li/LFP	GO	PAN/LiClO <sub>4</sub>	166 mAh/g after 50 cycles at 0.2 C and 60 °C	99	[143]	
Li/LiClO <sub>4</sub>	NMC532	PPC-SPE	over 300 cycles at 0.3 C	69.2	[144]	
Li/LiNi <sub>0.8</sub> Co <sub>0.15</sub> Al <sub>0.05</sub> O <sub>2</sub>	NSG	LiPF <sub>6</sub>	Initial discharge capacity at 200.0 mAh/g at 0.5 C	85	[18]	
Li/NCM622	2D BN	FPH-Li	over 300 stable cycles at 1 C	81.5	[146]	
Li/S	2D BN	Li <sub>7</sub> P <sub>3</sub> S <sub>11</sub>	185.4 mAh/g after 50 cycles at 1/20 C and room temperature	23	[148]	
Li/LFP	2D BN	PVDF-HFP/LiTFSI	116 mAh/g after 50 cycles at 0.2 C	76	[149]	
Li/Cu	2D BN	LiPF <sub>6</sub>	Coulomb efficiency stable at 92% over 100 cycles at 0.5 mA cm <sup>-2</sup>	–	[118]	
Li/Cu	h-BN	Organic carbonate	over 50 stable cycles at 2.0 mA cm <sup>-2</sup>	–	[150]	
Li/LFP	h-BN	PEO/LiTFSI	143.3 mAh/g after 140 cycles at 0.2 C and 60 °C	93	[151]	
Li/S	2D BN	PEO-PVDF	Initial reversible ratio capacity at 1200 mAh/g at 1/20 C	–	[152]	
Li/LFP	2D BN	BNP	over 600 cycles at 0.5 C and 25 °C	80	[153]	
Li/LFP	Ti <sub>3</sub> C <sub>2</sub> T <sub>x</sub>	PEO <sub>20</sub> -LiTFSI	over 100 cycles at 1/3 C and 60 °C	91.4	[159]	
Li/LiCoO <sub>2</sub>	MXene	M-HAP@PVHF	145 mAh/g after 150 cycles at 1 C	99	[162]	
Li/S	Ti <sub>3</sub> C <sub>2</sub> T <sub>x</sub>	Li <sub>2</sub> S <sub>6</sub>	800 mAh/g at 2C, over 1000 cycles at 2C	72	[167]	
Li/LFP	MnO <sub>2</sub>	PEO/LiTFSI	over 300 cycles at 0.5C and 60 °C	86.7	[59]	
Li/LFP	g-C <sub>3</sub> N <sub>4</sub>	PEO/LiTFSI	155 mAh/g after 100 cycles at 2C and 60 °C	96	[169]	

and battery performance improvement compared to 0D and 1D nano-filters [159]. In view of the same property, Ha et al. investigated the lithium-philic surface-guided lithium metal nucleation and growth behavior of LiTFSI in an electrolyte containing 2 wt% LiNO<sub>3</sub> in 1,3-dioxane/1,2-dimethoxyethane using oxygen/fluorine bifunctionalized Ti<sub>3</sub>C<sub>2</sub>T<sub>x</sub> MXene as a lithophilic substrate. The results show that the solid-solid interface between the lithophilic substrate and the inorganic SEI layer significantly reduces the nucleation overpotential and the surface tension of the lithium nuclei, and uniformly dispersed lithium nanoparticles are formed on the MXene substrate, which results in a high Coulombic efficiency and stable cycling performance (>1000 cycles) [160].

MXene as a filler can lower the glass transition temperature of SPE and promote the dissociation of metal ions, thus increasing the amount of free metal ions [161]. Hou et al. showed a significant enhancement of SPE ion transport by decorating poly (vinylidene fluoride-co-hexafluoropropylene) (PVHF) and hydroxyapatite nanowire networks (HAP) networks matrix. The resulting M-HAP@PVHF separator has high mechanical strength and effective flame retardancy, which results in a smoother SEI layer during cycling. Compared with the conventional polypropylene separator, the lithium symmetric battery assembled with M-HAP@PVHF diaphragm showed ~700 h stable plating/stripping cycles (Fig. 10b) [162]. Liu et al. also investigated the effect of Ti<sub>3</sub>C<sub>2</sub>T<sub>x</sub> fillers on the proton conductivity properties of polymer electrolyte membranes, represented by two typical polymers, Nafion and chitosan. The results showed that the 2D structure of Ti<sub>3</sub>C<sub>2</sub>T<sub>x</sub> helps to create remote proton transfer pathways along the interfacial domains (shown in Fig. 10c). Homogeneously dispersed Ti<sub>3</sub>C<sub>2</sub>T<sub>x</sub> on various composite membranes significantly enhanced the proton conductivity of the polymer membranes under hydrated or anhydrous conditions [163]. Meng et al. doped MXene into a fluorinated polymer matrix containing an ether-carbonate solvent blend and prepared a flame-retardant gel polymer electrolyte for dealing with the conflict between Li<sub>2</sub>S cathode and silicon anode in terms of electrolyte compatibility, while improving battery safety [164].

The termination of MXenes can be either determined by the synthesis process or controlled by post-processing [165]. Thus, the nature of MXene can be tuned by controlling the termination of MXene. In Li-S batteries, the termination of MXenes can promote strong chemical interactions with lips, allowing MXenes to act as sulfur hosts or intermediate layer materials between the positive electrode and the separator, thus mitigating the shuttle effect and improving the cycling stability of Li-S batteries [166]. Jiao et al. by preparing *in situ* TiO<sub>2</sub>-MXene (Ti<sub>3</sub>C<sub>2</sub>T<sub>x</sub>) heterostructure, a multifunctional catalyst with strong polysulfide adsorption capacity, excellent polysulfide conversion activity, high specific surface area and electronic conductivity was proposed. As

shown in Fig. 10d, the formed TiO<sub>2</sub> nanoparticles acted as adsorption centers to capture LiPSs, while the heterogeneous interface ensured the smooth diffusion of LiPSs from TiO<sub>2</sub> to MXene for further conversion. During the oxidation process, MXene flakes were partially converted to TiO<sub>2</sub> nanoparticles by controlled treatment while maintaining the 2D structure, high conductivity, and sufficient surface area to provide efficient LiPSs conversion [167].

### 5.5. Other 2D materials

In addition to the above, 2D materials composed of monoatomic layers also have excellent electrochemical, chemical, thermal and mechanical properties, which are widely used for the modification of solid lithium batteries [168]. Since MnO<sub>2</sub> can be combined with PEO chain, Li et al. selected MnO<sub>2</sub> nanosheet as filler to improve the electrochemical and mechanical properties of SPE. The capacity of solid lithium metal battery using PEO/MnO<sub>2</sub> composite SPE (143.5 mAh/g after 300 cycles) was higher than that of electrolyte without filler (61.2 mAh/g after 90 cycles) [59]. In addition, Sun et al. proposed using g-C<sub>3</sub>N<sub>4</sub> nanosheet as a new filler for PEO-based electrolyte, the addition of g-C<sub>3</sub>N<sub>4</sub> improved the electrical properties (ionic conductivity, lithium-ion transfer number and electrochemical window), mechanical properties and thermal stability of the composite electrolyte. The all-solid-state battery assembled by the g-C<sub>3</sub>N<sub>4</sub> composite electrolyte remained at 155 mAh/g after 100 cycles at 60 °C. This is due to the effective ion transport network formed by the 2D g-C<sub>3</sub>N<sub>4</sub> in the composite electrolyte. In addition, the surface atoms of g-C<sub>3</sub>N<sub>4</sub> interact with the groups in the lithium salt, promoting the further dissociation of lithium salt [169]. Table 3 summarizes the electrochemical properties of SSE modified with 2D materials.

## 6. Summary and outlook

Due to their advantages in safety and energy density, all-solid-state lithium metal batteries are currently the most promising option. However, natural interface defects have become a stumbling block to their development, including poor interfacial interactions and poor chemical/electrochemical stability. Most recent work has focused on electrode/electrolyte interface tuning, while the interface of SSE itself is a shortcoming and a key factor affecting battery performance. Based on the analysis of the structural characteristics of different SSEs and their inherent defects, the preparation methods of different 2D materials (MoS<sub>2</sub>, graphene and its oxides, BN, etc.) and the improvement pathways to modify the SSEs are reviewed. This work provides a basic reference for the development of subsequent 2D material modified all-solid-state lithium metal batteries.

Currently, there are numerous materials for modifying SSEs in all-

solid-state lithium metals, but the application of 2D materials for modifying SSEs is still in its infancy. In the future, there are still many significant challenges to be solved on the way to realize lithium metal as anode in all-solid-state batteries, such as relatively low lithium-ion conductivity, interfacial resistance, growth of lithium dendrites for side reactions, etc. In order to promote the further application of using 2D materials in all-solid-state lithium metal batteries, the disadvantages of solid-state batteries in terms of cycle stability and energy density need to be solved, and some 2D materials in solid-state are given below electrolyte applications are given below.

More advanced 2D materials need to be developed in the future, either by developing new heterogeneous structure of 2D materials or by modifying 2D materials to improve their chemical stability and mechanical strength, and the modified 2D materials can resolve the problem of low ionic conductivity of solid-state batteries at room temperature. In addition, given the excellent physicochemical properties of 2D materials, it may be a good choice to combine 2D materials with new materials to achieve a high-performance all-solid-state lithium metal battery. We believe that introducing 2D materials into all-solid-state batteries to form an all-2D material battery, where both the electrode and electrolyte can be tightly coupled with 2D materials, can resolve this problem in all-solid-state lithium metal batteries.

### Declaration of Competing Interest

The authors declare that they have no known competing financial interests or personal relationships that could have appeared to influence the work reported in this paper.

### Data availability

No data was used for the research described in the article.

### Acknowledgments

This work is supported by National Key R&D Program of China (No. 2022YFE0201300), Guangdong Basic and Applied Basic Research Foundation (Nos. 2022A1515110528, 2023A1515012792), New Faculty Startup Fund of China University of Geosciences (No. 162301212607), State Key Laboratory of Advanced Technology for Materials Synthesis and Processing (Wuhan University of Technology) (No. 2022-KF-24).

### References

- [1] J. Han, M.J. Lee, K. Lee, Y.J. Lee, S.H. Kwon, J.H. Min, E. Lee, W. Lee, S.W. Lee, B. J. Kim, Role of bicontinuous structure in elastomeric electrolytes for high-energy solid-state lithium-metal batteries, *Adv. Mater.* 35 (1) (2023), e2205194, <https://doi.org/10.1002/adma.202205194>.
- [2] Y. Gao, Z. Pan, J. Sun, Z. Liu, J. Wang, High-energy batteries: beyond lithium-ion and their long road to commercialisation, *Nano-Micro Lett.* 14 (1) (2022) 94, <https://doi.org/10.1007/s40820-022-00844-2>.
- [3] P. Shi, J. Ma, M. Liu, S. Guo, Y. Huang, S. Wang, L. Zhang, L. Chen, K. Yang, X. Liu, Y. Li, X. An, D. Zhang, X. Cheng, Q. Li, W. Lv, G. Zhong, Y.B. He, F. Kang, A dielectric electrolyte composite with high lithium-ion conductivity for high-voltage solid-state lithium metal batteries, *Nat. Nanotechnol.* 18 (6) (2023) 602–610, <https://doi.org/10.1038/s41565-023-01341-2>.
- [4] A. Kondori, M. Esmaeilrad, A.M. Harzandi, R. Amine, M.T. Saray, L. Yu, T. Liu, J. Wen, N. Shan, H.H. Wang, A.T. Ngo, P.C. Redfern, C.S. Johnson, K. Amine, R. Shahbazian Yassar, L.A. Curtiss, M. Asadi, A room temperature rechargeable  $\text{Li}_2\text{O}$ -based lithium-air battery enabled by a solid electrolyte, *Science* 379 (6631) (2023) 499–505, <https://doi.org/10.1126/science.abq1347>.
- [5] C. Sun, J. Liu, Y. Gong, D.P. Wilkinson, J. Zhang, Recent advances in all-solid-state rechargeable lithium batteries, *Nano Energy* 33 (2017) 363–386, <https://doi.org/10.1016/j.nanoen.2017.01.028>.
- [6] F. Zheng, M. Kotobuki, S. Song, M.O. Lai, L. Lu, Review on solid electrolytes for all-solid-state lithium-ion batteries, *J. Power Sources* 389 (2018) 198–213, <https://doi.org/10.1016/j.jpowsour.2018.04.022>.
- [7] P. Sayavong, W. Zhang, S.T. Oyakhire, D.T. Boyle, Y. Chen, S.C. Kim, R.A. Vilá, S. E. Holmes, M.S. Kim, S.F. Bent, Z. Bao, Y. Cui, Dissolution of the solid electrolyte interphase and its effects on lithium metal anode cyclability, *J. Am. Chem. Soc.* 145 (22) (2023) 12342–12350, <https://doi.org/10.1021/jacs.3c03195>.
- [8] M.D. Tikekar, S. Choudhury, Z. Tu, L.A. Archer, Design principles for electrolytes and interfaces for stable lithium-metal batteries, *Nat. Energy* 1 (9) (2016) 1–7, <https://doi.org/10.1038/nenergy.2016.114>.
- [9] X. Yu, A. Manthiram, Electrode-electrolyte interfaces in lithium-based batteries, *Energy Environ. Sci.* 11 (3) (2018) 527–543, <https://doi.org/10.1039/c7ee02555f>.
- [10] P. Molaiyan, S.E. Mailhiot, K. Voges, A.M. Kantola, T. Hu, P. Michalowski, A. Kwade, V.-V. Telkki, U. Lassi, Investigation of the structure and ionic conductivity of a  $\text{Li}_3\text{InCl}_6$  modified by dry room annealing for solid-state Li-ion battery applications, *Mater. Des.* 227 (2023), 111690, <https://doi.org/10.1016/j.matedes.2023.111690>.
- [11] Q. Ma, Y. Zheng, D. Luo, T. Or, Y. Liu, L. Yang, H. Dou, J. Liang, Y. Nie, X. Wang, A. Yu, Z. Chen, 2D materials for all-solid-state lithium batteries, *Adv. Mater.* 34 (16) (2022), e2108079, <https://doi.org/10.1002/adma.202108079>.
- [12] Y. Mo, L. Liao, D. Li, R. Pan, Y. Deng, Y. Tan, H. Zhou, Development prospects of metal-based two-dimensional nanomaterials in lithium-sulfur batteries, *Chin. Chem. Lett.* 34 (1) (2023), 107130, <https://doi.org/10.1016/j.ccl.2022.01.023>.
- [13] L. Peng, Y. Zhu, D. Chen, R.S. Ruoff, G. Yu, Two-dimensional materials for beyond-lithium-ion batteries, *Adv. Energy Mater.* 6 (11) (2016), 1600025, <https://doi.org/10.1002/aemn.201600025>.
- [14] R. Rojaee, R. Shahbazian Yassar, Two-dimensional materials to address the lithium battery challenges, *ACS Nano* 14 (3) (2020) 2628–2658, <https://doi.org/10.1021/acsnano.9b08396>.
- [15] C. Guo, H. Li, W. Zhao, J. Pan, T. Lin, J. Xu, M. Chen, F. Huang, High-quality single-layer nanosheets of  $\text{MS}_2$ (M = Mo, Nb, Ta, Ti) directly exfoliated from  $\text{AMS}_2$ (A = Li, Na, K) crystals, *J. Mater. Chem. C* 5 (24) (2017) 5977–5983, <https://doi.org/10.1039/c7tc00838d>.
- [16] E. Gao, S. Lin, Z. Qin, M.J. Buehler, X. Feng, Z. Xu, Mechanical exfoliation of two-dimensional materials, *J. Mech. Phys. Solids* 115 (2018) 248–262, <https://doi.org/10.1016/j.jmps.2018.03.014>.
- [17] Q. Ji, Y. Zhang, Y. Zhang, Z. Liu, Chemical vapour deposition of group-VIB metal dichalcogenide monolayers: engineered substrates from amorphous to single crystalline, *Chem. Soc. Rev.* 44 (9) (2015) 2587–2602, <https://doi.org/10.1039/c4cs00258j>.
- [18] W.K. Shin, A.G. Kannan, D.W. Kim, Effective suppression of dendritic lithium growth using an ultrathin coating of nitrogen and sulfur codoped graphene nanosheets on polymer separator for lithium metal batteries, *ACS Appl. Mater. Interfaces* 7 (42) (2015) 23700–23707, <https://doi.org/10.1021/acsm.5b07730>.
- [19] E. Cha, M.D. Patel, J. Park, J. Hwang, V. Prasad, K. Cho, W. Choi, 2D  $\text{MoS}_2$  as an efficient protective layer for lithium metal anodes in high-performance Li-S batteries, *Nat. Nanotechnol.* 13 (4) (2018) 337–344, <https://doi.org/10.1038/s41565-018-0061-y>.
- [20] W. Zhao, J. Yi, P. He, H. Zhou, Solid-state electrolytes for lithium-ion batteries: Fundamentals, challenges and perspectives, *Electrochim. Energy Rev.* 2 (4) (2019) 574–605, <https://doi.org/10.1007/s41918-019-00048-0>.
- [21] J.S. Kim, G. Yoon, S. Kim, S. Sugata, N. Yashiro, S. Suzuki, M.J. Lee, R. Kim, M. Badding, Z. Song, J.M. Chang, D. Im, Surface engineering of inorganic solid-state electrolytes via interlayers strategy for developing long-cycling quasi-all-solid-state lithium batteries, *Nat. Commun.* 14 (1) (2023) 782, <https://doi.org/10.1038/s41467-023-36401-7>.
- [22] X. Yang, J. Liu, N. Pei, Z. Chen, R. Li, L. Fu, P. Zhang, J. Zhao, The critical role of fillers in composite polymer electrolytes for lithium battery, *Nano-Micro Lett.* 15 (1) (2023) 74, <https://doi.org/10.1007/s40820-023-01051-3>.
- [23] J.B. Goodenough, H.Y.P. Hong, J.A. Kafalas, Fast  $\text{Na}^+$ -ion transport in skeleton structures, *Mater. Res. Bull.* 11 (2) (1976) 203–220, <https://doi.org/10.1126/sciadv.aax5587>.
- [24] H. Aono, E. Sugimoto, Y. Sadaaka, N. Imanaka, G. Adachi, Ionic conductivity and sinter ability of lithium titanium phosphate system, *Solid State Ion.* 40–41 (1990) 38–42, [https://doi.org/10.1016/0167-2738\(90\)90282-v](https://doi.org/10.1016/0167-2738(90)90282-v).
- [25] W. Xiao, J. Wang, L. Fan, J. Zhang, X. Li, Recent advances in  $\text{Li}_{1+x}\text{Al}_x\text{Ti}_{2-x}\text{PO}_4$ <sub>3</sub> solid-state electrolyte for safe lithium batteries, *Energy Storage Mater.* 19 (2019) 379–400, <https://doi.org/10.1016/j.ensm.2018.10.012>.
- [26] M. Hou, F. Liang, K. Chen, Y. Dai, D. Xue, Challenges and perspectives of NASICON-type solid electrolytes for all-solid-state lithium batteries, *Nanotechnology* 31 (13) (2020), 132003, <https://doi.org/10.1088/1361-6528/ab5be7>.
- [27] S. He, Y. Xu, B. Zhang, X. Sun, Y. Chen, Y. Jin, Unique rhombus-like precursor for synthesis of  $\text{Li}_{1.3}\text{Al}_{0.3}\text{Ti}_{1.7}(\text{PO}_4)_3$  solid electrolyte with high ionic conductivity, *Chem. Eng. J.* 345 (2018) 483–491, <https://doi.org/10.1016/j.cej.2018.03.151>.
- [28] J. Feng, Z. Gao, L. Sheng, Z. Hao, F.R. Wang, Progress and perspective of interface design in garnet electrolyte-based all-solid-state batteries, *Carbon Energy* 3 (3) (2021) 385–409, <https://doi.org/10.1002/cey.2100>.
- [29] V. Thangadurai, H. Kaack, W.J.F. Weppner, Novel fast lithium ion conduction in garnet-type  $\text{Li}_5\text{La}_3\text{Zr}_2\text{O}_{12}$  (M = Nb, Ta), *J. Am. Ceram. Soc.* 86 (3) (2003) 437–440, <https://doi.org/10.1111/j.1151-2916.2003.tb03318.x>.
- [30] R. Murugan, V. Thangadurai, W. Weppner, Fast lithium ion conduction in garnet-type  $\text{Li}_7\text{La}_3\text{Zr}_2\text{O}_{12}$ , *Angew. Chem. Int. Ed. Engl.* 46 (41) (2007) 7778–7781, <https://doi.org/10.1002/anie.200701144>.
- [31] J. Huang, F. Liang, M. Hou, Y. Zhang, K. Chen, D. Xue, Garnet-type solid-state electrolytes and interfaces in all-solid-state lithium batteries: progress and perspective, *Appl. Mater. Today* 20 (2020), 100750, <https://doi.org/10.1016/j.apmt.2020.100750>.
- [32] A.J. Samson, K. Hofstetter, S. Bag, V. Thangadurai, A bird's-eye view of Li-stuffed garnet-type  $\text{Li}_7\text{La}_3\text{Zr}_2\text{O}_{12}$  ceramic electrolytes for advanced all-solid-state Li

- batteries, *Energy Environ. Sci.* 12 (10) (2019) 2957–2975, <https://doi.org/10.1039/c9ee01548e>.
- [33] J. Lu, Y. Li, Perovskite-type Li-ion solid electrolytes: A review, *J. Mater. Sci.: Mater. Electron.* 32 (8) (2021) 9736–9754, <https://doi.org/10.1007/s10854-021-05699-8>.
- [34] C.L. Yoshiyuki Inaguma, M. Itoh, TetsurB Nakamura, High ionic conductivity in lithium lanthanum titanate, *Solid-State Commun.* 86 (10) (1993) 689–693, [https://doi.org/10.1016/0038-1098\(93\)90841-a](https://doi.org/10.1016/0038-1098(93)90841-a).
- [35] S. Stramare, V. Thangadurai, W. Weppner, Lithium lanthanum titanates: A review, *Chem. Mater.* 15 (2003) 3974–3990, <https://doi.org/10.1021/cm0300516>.
- [36] D. Wang, L. Jhang, R. Kou, M. Liao, S. Zheng, H. Jiang, P. Shi, G.-X. Li, K. Meng, D. Wang, Realizing high-capacity all-solid-state lithium-sulfur batteries using a low-density inorganic solid-state electrolyte, *Nat. Commun.* 14 (1) (2023) 1895, <https://doi.org/10.1038/s41467-023-37564-z>.
- [37] J. Wu, S. Liu, F. Han, X. Yao, C. Wang, Lithium/Sulfide all-solid-state batteries using sulfide electrolytes, *Adv. Mater.* 33 (6) (2021), e2000751, <https://doi.org/10.1002/adma.202000751>.
- [38] D. Lei, K. Shi, H. Ye, Z. Wan, Y. Wang, L. Shen, B. Li, Q.H. Yang, F. Kang, Y.B. He, Progress and perspective of solid-state lithium-sulfur batteries, *Adv. Funct. Mater.* 28 (38) (2018), 1707570, <https://doi.org/10.1002/adfm.201707570>.
- [39] N. Kamaya, K. Homma, Y. Yamakawa, M. Hirayama, R. Kanno, M. Yonemura, T. Kamiyama, Y. Kato, S. Hama, K. Kawamoto, A. Mitsui, A lithium superionic conductor, *Nat. Mater.* 10 (9) (2011) 682–686, <https://doi.org/10.1038/nmat3066>.
- [40] D.E. Fenton, J.M. Parker, P.V. Wright, Complexes of alkali metal ions with poly (ethylene oxide), *Polymer* 14 (11) (1973), 589, [https://doi.org/10.1016/0032-3861\(73\)90146-8](https://doi.org/10.1016/0032-3861(73)90146-8).
- [41] Z. Cheng, T. Liu, B. Zhao, F. Shen, H. Jin, X. Han, Recent advances in organic-inorganic composite solid electrolytes for all-solid-state lithium batteries, *Energy Storage Mater.* 34 (2021) 388–416, <https://doi.org/10.1016/j.ensm.2020.09.016>.
- [42] W.H. Meyer, Polymer electrolytes for lithium-ion batteries, *Adv. Mater.* 10 (6) (1998) 439–448, [https://doi.org/10.1002/\(sici\)1521-4095\(199804\)10:6<439::aid-adma439>3.0.co;2-i](https://doi.org/10.1002/(sici)1521-4095(199804)10:6<439::aid-adma439>3.0.co;2-i).
- [43] Y. Tominaga, K. Yamazaki, Fast Li-ion conduction in poly(ethylene carbonate)-based electrolytes and composites filled with TiO<sub>2</sub> nanoparticles, *Chem. Commun.* 50 (34) (2014) 4448–4450, <https://doi.org/10.1039/c3cc49588d>.
- [44] Y. Su, F. Xu, X. Zhang, Y. Qiu, H. Wang, Rational design of high-performance PEO/ceramic composite solid electrolytes for lithium metal batteries, *Nano-Micro Lett.* 15 (1) (2023) 82, <https://doi.org/10.1007/s40820-023-01055-z>.
- [45] L. Li, Y. Deng, G. Chen, Status and prospect of garnet/polymer solid composite electrolytes for all-solid-state lithium batteries, *J. Energy Chem.* 50 (2020) 154–177, <https://doi.org/10.1016/j.jecchem.2020.03.017>.
- [46] C. Liang, Z. Gu, Y. Zhang, Z. Ma, H. Qiu, J. Gu, Structural design strategies of polymer matrix composites for electromagnetic interference shielding: A review, *Nano-Micro Lett.* 13 (1) (2021) 181, <https://doi.org/10.1007/s40820-021-00707-2>.
- [47] Y. An, X. Han, Y. Liu, A. Azhar, J. Na, A.K. Nanjundan, S. Wang, J. Yu, Y. Yamauchi, Progress in solid polymer electrolytes for lithium-ion batteries and beyond, *Small* 18 (3) (2022), e2103617, <https://doi.org/10.1002/smll.202103617>.
- [48] Y. Hu, N. Dunlap, S. Wan, S. Lu, S. Huang, I. Sellinger, M. Ortiz, Y. Jin, S.H. Lee, W. Zhang, Crystalline lithium imidazolate covalent organic frameworks with high Li-ion conductivity, *J. Am. Chem. Soc.* 141 (18) (2019) 7518–7525, <https://doi.org/10.1021/jacs.9b02448>.
- [49] H. Chen, Q.Y. Liu, M.X. Jing, F. Chen, W.Y. Yuan, B.W. Ju, F.Y. Tu, X.Q. Shen, S. B. Qin, Improved interface stability and room-temperature performance of solid-state lithium batteries by integrating cathode/electrolyte and graphite coating, *ACS Appl. Mater. Interfaces* 12 (13) (2020) 15120–15127, <https://doi.org/10.1021/acsmami.9b22690>.
- [50] L.X. Li, R. Li, Z.H. Huang, H. Yang, M.Q. Liu, J. Xiang, S. Hussain, X.Q. Shen, M. X. Jing, A multifunctional gradient solid electrolyte remarkably improving interface compatibility and ion transport in solid-state lithium battery, *ACS Appl. Mater. Interfaces* 14 (27) (2022) 30786–30795, <https://doi.org/10.1021/acsmami.2c05578>.
- [51] H. Yang, M. Jing, H. Li, W. Yuan, B. Deng, Q. Liu, B. Ju, X. Zhang, S. Hussain, X. Shen, X. Yan, 'Environment-friendly' polymer solid electrolyte membrane via a rapid surface-initiating polymerization strategy, *Chem. Eng. J.* 421 (2021), 129710, <https://doi.org/10.1016/j.cej.2021.129710>.
- [52] H. Yang, B. Zhang, M. Jing, X. Shen, L. Wang, H. Xu, X. Yan, X. He, In situ catalytic polymerization of a highly homogeneous PDOL composite electrolyte for long-cycle high-voltage solid-state lithium batteries, *Adv. Energy Mater.* 12 (39) (2022), <https://doi.org/10.1002/aenm.202201762>.
- [53] S. Li, S.Q. Zhang, L. Shen, Q. Liu, J.B. Ma, W. Lv, Y.B. He, Q.H. Yang, Progress and perspective of ceramic/polymer composite solid electrolytes for lithium batteries, *Adv. Sci.* 7 (5) (2020), 1903088, <https://doi.org/10.1002/advs.201903088>.
- [54] J. Liang, J. Luo, Q. Sun, X. Yang, R. Li, X. Sun, Recent progress on solid-state hybrid electrolytes for solid-state lithium batteries, *Energy Storage Mater.* 21 (2019) 308–334, <https://doi.org/10.1016/j.jensm.2019.06.021>.
- [55] M. Dirican, C. Yan, P. Zhu, X. Zhang, Composite solid electrolytes for all-solid-state lithium batteries, *Mater. Sci. Eng.: R.* 136 (2019) 27–46, <https://doi.org/10.1016/j.mser.2018.10.004>.
- [56] X. Zhao, Z. Zhang, X. Zhang, B. Tang, Z. Xie, Z. Zhou, Computational screening and first-principles investigations of NASICON-type Li<sub>x</sub>M<sub>2</sub>(PO<sub>4</sub>)<sub>3</sub> as solid electrolytes for Li batteries, *J. Mater. Chem. A* 6 (6) (2018) 2625–2631, <https://doi.org/10.1039/c7ta08968f>.
- [57] K. Yang, L. Chen, J. Ma, Y.B. He, F. Kang, Progress and perspective of Li<sub>1+x</sub>AlTi<sub>2-x</sub>(PO<sub>4</sub>)<sub>3</sub> ceramic electrolyte in lithium batteries, *InfoMat* 3 (11) (2021) 1195–1217, <https://doi.org/10.1002/inf2.12222>.
- [58] H. Huo, J. Luo, V. Thangadurai, X. Guo, C. Nan, X. Sun, Li<sub>2</sub>CO<sub>3</sub>: A critical issue for developing solid garnet batteries, *ACS Energy Lett.* 5 (1) (2019) 252–262, <https://doi.org/10.1021/acsenergylett.9b02401>.
- [59] S. Song, Y. Wu, Z. Dong, F. Deng, W. Tang, J. Yao, Z. Wen, L. Lu, N. Hu, J. Molenda, Multi-substituted garnet-type electrolytes for solid-state lithium batteries, *Ceram. Int.* 46 (4) (2020) 5489–5494, <https://doi.org/10.1016/j.ceramint.2019.10.290>.
- [60] J. Dai, C. Yang, C. Wang, G. Pastel, L. Hu, Interface engineering for garnet-based solid-state lithium-metal batteries: materials, structures, and characterization, *Adv. Mater.* 30 (48) (2018), e1802068, <https://doi.org/10.1002/adma.201802068>.
- [61] M. Kim, I.W. Choi, S.J. Choi, J.W. Song, S.I. Mo, J.H. An, Y. Jo, S. Ahn, S.K. Ahn, G.H. Kim, D.S. Kim, Enhanced electrical properties of Li-salts doped mesoporous TiO<sub>2</sub> in perovskite solar cells, *Joule* 5 (3) (2021) 659–672, <https://doi.org/10.1016/j.joule.2021.02.007>.
- [62] W.J. Kwon, H. Kim, K.-N. Jung, W. Cho, S.H. Kim, J.-W. Lee, M.-S. Park, Enhanced Li<sup>+</sup> conduction in perovskite Li<sub>3</sub>La<sub>2/3-x</sub>□<sub>1/3-x</sub>TiO<sub>3</sub> solid-electrolytes via microstructural engineering, *J. Mater. Chem. A* 5 (13) (2017) 6257–6262, <https://doi.org/10.1039/c7ta00196g>.
- [63] Y. Liu, P. He, H. Zhou, Rechargeable solid-state Li-air and Li-S batteries: Materials, construction, and challenges, *Adv. Energy Mater.* 8 (4) (2018), 1701602, <https://doi.org/10.1002/aenm.201701602>.
- [64] A.K. Kenessova, G.A. Seilkhanova, T.S. Kurmabayeva, E.Z. Ussipbekova, A. P. Kurbatov, Solid polymer electrolytes for energy storage systems, *Mater. Today: Proc.* 31 (2020) 588–591, <https://doi.org/10.1016/j.matr.2020.07.106>.
- [65] G. Xi, M. Xiao, S. Wang, D. Han, Y. Li, Y. Meng, Polymer-based solid electrolytes: Material selection, design, and application, *Adv. Funct. Mater.* 31 (9) (2020), 2007598, <https://doi.org/10.1002/adfm.202007598>.
- [66] N.S. Grundish, J.B. Goodenough, H. Khani, Designing composite polymer electrolytes for all-solid-state lithium batteries, *Curr. Opin. Electrochem.* 30 (2021), 100828, <https://doi.org/10.1016/j.coelec.2021.100828>.
- [67] M. Yang, Y. Liu, Y. Mo, Lithium crystallization at solid interfaces, *Nat. Commun.* 14 (1) (2023) 2986, <https://doi.org/10.1038/s41467-023-38757-2>.
- [68] X. Miao, S. Guan, C. Ma, L. Li, C.W. Nan, Role of interfaces in solid-state batteries, *Adv. Mater.* (2022), e2206402, <https://doi.org/10.1002/adma.202206402>.
- [69] Y. Xiao, Y. Wang, S.H. Bo, J.C. Kim, L.J. Miara, G. Ceder, Understanding interface stability in solid-state batteries, *Nat. Rev. Mater.* 5 (2) (2019) 105–126, <https://doi.org/10.1038/s41578-019-0157-5>.
- [70] Y. Wang, Separator wettability enhanced by electrolyte additive to boost the electrochemical performance of lithium metal batteries, *Nano-Micro Lett.* 13 (1) (2021) 210, <https://doi.org/10.1007/s40820-021-00731-2>.
- [71] T. Liu, J. Wang, Y. Xu, Y. Zhang, Y. Wang, Dendrite-free and stable lithium metal battery achieved by a model of stepwise lithium deposition and stripping, *Nano-Micro Lett.* 13 (1) (2021) 170, <https://doi.org/10.1007/s40820-021-00687-3>.
- [72] Y. Sun, Q. Zhang, L. Yan, T. Wang, P. Hou, A review of interfaces within solid-state electrolytes: fundamentals, issues and advancements, *Chem. Eng. J.* 437 (2022), 135179, <https://doi.org/10.1016/j.cej.2022.135179>.
- [73] X. Xu, S. Wang, Y. Zhao, H. Li, Interface optimization in solid-state lithium batteries, *J. Chin. Ceram. Soc.* 49 (7) (2021) 1466–1484, <https://doi.org/10.14062/j.issn.0454-5648.20200664>.
- [74] X. Chen, Z. Guan, F. Chu, Z. Xue, F. Wu, Y. Yu, Air-stable inorganic solid-state electrolytes for high energy density lithium batteries: Challenges, strategies, and prospects, *InfoMat* 4 (1) (2021), e12248, <https://doi.org/10.1002/inf2.12248>.
- [75] C. Wang, J.T. Kim, C. Wang, X. Sun, Progress and prospects of inorganic solid-state electrolyte-based all-solid-state pouch cells, *Adv. Mater.* 35 (19) (2023), e2209074, <https://doi.org/10.1002/adma.202209074>.
- [76] Q. Zhao, S. Stalin, C.Z. Zhao, L.A. Archer, Designing solid-state electrolytes for safe, energy-dense batteries, *Nat. Rev. Mater.* 5 (3) (2020) 229–252, <https://doi.org/10.1038/s41578-019-0165-5>.
- [77] J. Wu, L. Yuan, W. Zhang, Z. Li, X. Xie, Y. Huang, Reducing the thickness of solid-state electrolyte membranes for high-energy lithium batteries, *Energy Environ. Sci.* 14 (1) (2021) 12–36, <https://doi.org/10.1039/D0EE02241A>.
- [78] S. Liu, W. Liu, D. Ba, Y. Zhao, Y. Ye, Y. Li, J. Liu, Filler-integrated composite polymer electrolyte for solid-state lithium batteries, *Adv. Mater.* 35 (2) (2023) 2110423, <https://doi.org/10.1002/adma.202110423>.
- [79] L. Zhang, Y. Liu, Y. You, A. Vinu, L. Mai, NASICONs-type solid-state electrolytes: The history, physicochemical properties, and challenges, *Interdisc. Mater.* 2 (1) (2022) 91–110, <https://doi.org/10.1002/idm2.12046>.
- [80] X. Han, Y. Gong, K. Fu, X. He, G.T. Hitz, J. Dai, A. Pearse, B. Liu, H. Wang, G. Rubloff, Y. Mo, V. Thangadurai, E.D. Wachsman, L. Hu, Negating interfacial impedance in garnet-based solid-state Li metal batteries, *Nat. Mater.* 16 (5) (2017) 572–579, <https://doi.org/10.1038/nmat4821>.
- [81] Z. Zhang, Q. Zhang, J. Shi, Y.S. Chu, X. Yu, K. Xu, M. Ge, H. Yan, W. Li, L. Gu, Y. Hu, H. Li, X. Yang, L. Chen, X. Huang, A self-forming composite electrolyte for solid-state sodium battery with ultralong cycle life, *Adv. Energy Mater.* 7 (4) (2017), 1601196, <https://doi.org/10.1002/aenm.201601196>.
- [82] P. Jiang, G. Du, J. Cao, X. Zhang, C. Zou, Y. Liu, X. Lu, Solid-state Li ion batteries with oxide solid electrolytes: Progress and perspective, *Energy Technol.* 11 (3) (2023), 2201288, <https://doi.org/10.1002/ente.202201288>.
- [83] K.K. Fu, Y. Gong, B. Liu, Y. Zhu, S. Xu, Y. Yao, W. Luo, C. Wang, S.D. Lacey, J. Dai, Y. Chen, Y. Mo, E. Wachsman, L. Hu, Toward garnet electrolyte-based Li metal

- batteries: An ultrathin, highly effective, artificial solid-state electrolyte/metallic Li interface, *Sci. Adv.* 3 (4) (2017), e1601659, <https://doi.org/10.1126/sciadv.1601659>.
- [84] J. Lou, G. Wang, Y. Xia, C. Liang, H. Huang, Y. Gan, X. Tao, J. Zhang, W. Zhang, Achieving efficient and stable interface between metallic lithium and garnet-type solid electrolyte through a thin indium tin oxide interlayer, *J. Power Sources* 448 (2020), 227440, <https://doi.org/10.1016/j.jpowsour.2019.227440>.
- [85] S. Chen, D. Xie, G. Liu, J.P. Mwizerwa, Q. Zhang, Y. Zhao, X. Xu, X. Yao, Sulfide solid electrolytes for all-solid-state lithium batteries: Structure, conductivity, stability and application, *Energy Storage Mater.* 14 (2018) 58–74, <https://doi.org/10.1016/j.jensm.2018.02.020>.
- [86] F. Han, J. Yue, X. Zhu, C. Wang, Suppressing Li dendrite formation in  $\text{Li}_2\text{S}-\text{P}_2\text{S}_5$  solid electrolyte by Li incorporation, *Adv. Energy Mater.* 8 (18) (2018), 1703644, <https://doi.org/10.1002/aenm.201703644>.
- [87] A. Kato, A. Hayashi, M. Tatsumisago, Enhancing utilization of lithium metal electrodes in all-solid-state batteries by interface modification with gold thin films, *J. Power Sources* 309 (2016) 27–32, <https://doi.org/10.1016/j.jpowsour.2016.01.068>.
- [88] Z. Ji, L. Feng, Z. Zhu, X. Fu, W. Yang, Y. Wang, Polymeric interface engineering in lithium-sulfur batteries, *Chem. Eng. J.* 455 (2023), 140462, <https://doi.org/10.1016/j.cej.2022.140462>.
- [89] X. Yuan, C. Sun, J.N. Duan, J. Fan, R. Yuan, J. Chen, J.K. Chang, M. Zheng, Q. Dong, A polyoxometalate-based polymer electrolyte with an improved electrode interface and ion conductivity for high-safety all-solid-state batteries, *J. Mater. Chem. A* 7 (26) (2019) 15924–15932, <https://doi.org/10.1039/c9ta04714j>.
- [90] H.F. Liu, S.L. Wong, D.Z. Chi, CVD growth of  $\text{MoS}_2$ -based two-dimensional materials, *Chem. Vap. Dep.* 21 (10-11-12) (2015) 241–259, <https://doi.org/10.1002/cvd.201500060>.
- [91] N.K. Perkgoz, M. Bay, Investigation of single-wall  $\text{MoS}_2$  monolayer flakes grown by chemical vapor deposition, *Nanomicro Lett.* 8 (1) (2016) 70–79, <https://doi.org/10.1007/s40820-015-0064-2>.
- [92] J. Wang, Z. Ren, Y. Hou, X. Yan, P. Liu, H. Zhang, H. Zhang, J. Guo, A review of graphene synthesis at low temperatures by CVD methods, *New Carbon Mater.* 35 (3) (2020) 193–208, [https://doi.org/10.1016/s1872-5805\(20\)60484-x](https://doi.org/10.1016/s1872-5805(20)60484-x).
- [93] D. Wei, S. Haque, P. Andrew, J. Kivioja, T. Ryhänen, A. Pesquera, A. Centeno, B. Alonso, A. Chuvilin, Ultrathin rechargeable all-solid-state batteries based on monolayer graphene, *J. Mater. Chem. A* 1 (9) (2013) 3177, <https://doi.org/10.1039/c3ta01183f>.
- [94] E. Matios, H. Wang, C. Wang, X. Hu, X. Lu, J. Luo, W. Li, Graphene regulated ceramic electrolyte for solid-state sodium metal battery with superior electrochemical stability, *ACS Appl. Mater. Interfaces* 11 (5) (2019) 5064–5072, <https://doi.org/10.1021/acsmami.8b19519>.
- [95] Q. Cheng, A. Li, N. Li, S. Li, A. Zangiabadi, T.D. Li, W. Huang, A.C. Li, T. Jin, Q. Song, W. Xu, N. Ni, H. Zhai, M. Dointigny, K. Zaghib, X. Chuan, D. Su, K. Yan, Y. Yang, Stabilizing solid electrolyte-anode interface in Li-metal batteries by boron nitride-based nanocomposite coating, *Joule* 3 (6) (2019) 1510–1522, <https://doi.org/10.1016/j.joule.2019.03.022>.
- [96] K. Kim, A. Hsu, X. Jia, S. Kim, Y. Shi, M. Dresselhaus, T. Palacios, J. Kong, Synthesis and characterization of hexagonal boron nitride film as a dielectric layer for graphene devices, *ACS Nano* 6 (10) (2012) 8583–8590, <https://doi.org/10.1021/nn301675f>.
- [97] W. Luo, Y. Gong, Y. Zhu, K.K. Fu, J. Dai, S.D. Lacey, C. Wang, B. Liu, X. Han, Y. Mo, E.D. Wachsman, L. Hu, Transition from superlithiophobicity to superlithiophilicity of garnet solid-state electrolyte, *J. Am. Chem. Soc.* 138 (37) (2016) 12258–12262, <https://doi.org/10.1021/jacs.6b06777>.
- [98] H. Ci, J. Cai, H. Ma, Z. Shi, G. Cui, M. Wang, J. Jin, N. Wei, C. Lu, W. Zhao, J. Sun, Z. Liu, Defective  $\text{VSe}_2$ -graphene heterostructures enabling *in situ* electrocatalyst evolution for lithium-sulfur batteries, *ACS Nano* 14 (9) (2020) 11929–11938, <https://doi.org/10.1021/acsnano.0c05030>.
- [99] Z. Hu, Z. Liu, J. Tian, Stacking of exfoliated two-dimensional materials: A review, *Chin. J. Chem.* 38 (9) (2020) 981–995, <https://doi.org/10.1002/cjoc.202000092>.
- [100] F. Xie, C. Xu, Y. Song, Q. Liang, J. Ji, S. Wang, 2D–2D heterostructure of ionic liquid-exfoliated  $\text{MoS}_2/\text{MXene}$  as lithium polysulfide barrier for Li-S batteries, *J. Colloid Interface Sci.* 636 (2023) 528–536, <https://doi.org/10.1016/j.jcis.2023.01.031>.
- [101] W.J. Hyun, C.M. Thomas, N.S. Luu, M.C. Hersam, Layered heterostructure ionogel electrolytes for high-performance solid-state lithium-ion batteries, *Adv. Mater.* 33 (13) (2021), e2007864, <https://doi.org/10.1002/adma.202007864>.
- [102] B. Shen, T.W. Zhang, Y.C. Yin, Z.X. Zhu, L.L. Lu, C. Ma, F. Zhou, H.B. Yao, Chemically exfoliated boron nitride nanosheets form robust interfacial layers for stable solid-state Li metal batteries, *Chem. Commun.* 55 (53) (2019) 7703–7706, <https://doi.org/10.1039/c9cc02124h>.
- [103] S. Xia, B. Yang, H. Zhang, J. Yang, W. Liu, S. Zheng, Ultrathin layered double hydroxide nanosheets enabling composite polymer electrolyte for all-solid-state lithium batteries at room temperature, *Adv. Funct. Mater.* 31 (28) (2021), 2101168, <https://doi.org/10.1002/adfm.202101168>.
- [104] W. Tang, S. Tang, C. Zhang, Q. Ma, Q. Xiang, Y. Yang, J. Luo, Simultaneously enhancing the thermal stability, mechanical modulus, and electrochemical performance of solid polymer electrolytes by incorporating 2D sheets, *Adv. Energy Mater.* 8 (24) (2018), 1800866, <https://doi.org/10.1002/aenm.201800866>.
- [105] K.S. Novoselov, A.K. Geim, S.V. Morozov, D. Jiang, Y. Zhang, S.V. Dubonos, I. V. Grigorieva, A.A. Firsov, Electric field effect in atomically thin carbon films, *Science* 306 (5696) (2004) 666–669, <https://doi.org/10.1126/science.1102896>.
- [106] Z. Sun, A. Martinez, F. Wang, Optical modulators with 2D layered materials, *Nat. Photon.* 10 (4) (2016) 227–238, <https://doi.org/10.1038/nphoton.2016.15>.
- [107] M.A.M. Hasan, Y. Wang, C.R. Bowen, Y. Yang, 2D nanomaterials for effective energy scavenging, *Nano-Micro Lett.* 13 (1) (2021) 82, <https://doi.org/10.1007/s40820-021-00603-9>.
- [108] W. Choi, N. Choudhary, G.H. Han, J. Park, D. Akinwande, Y.H. Lee, Recent development of two-dimensional transition metal dichalcogenides and their applications, *Mater. Today* 20 (3) (2017) 116–130, <https://doi.org/10.1016/j.mattod.2016.10.002>.
- [109] Y. Wu, D. Li, C.L. Wu, H.Y. Hwang, Y. Cui, Electrostatic gating and intercalation in 2D materials, *Nat. Rev. Mater.* 8 (1) (2023) 41–53, <https://doi.org/10.1038/s41578-022-00473-6>.
- [110] Z. Peng, R. Lin, Z. Li, L. Xu, X. Yu, X. Huang, W. Shi, X. He, X. Meng, L. Tong, X. Miao, L. Ye, Two-dimensional materials-based integrated hardware, *Sci. China Inf. Sci.* 66 (6) (2023), 160401, <https://doi.org/10.1007/s11432-023-3744-2>.
- [111] Q. Shao, Z.S. Wu, J. Chen, Two-dimensional materials for advanced Li-S batteries, *Energy Storage Mater.* 22 (2019) 284–310, <https://doi.org/10.1016/j.ensm.2019.02.001>.
- [112] S. Zheng, W. Zhao, J. Chen, X. Zhao, Z. Pan, X. Yang, 2D materials boost advanced Zn anodes: Principles, advances, and challenges, *Nano-Micro Lett.* 15 (1) (2023) 46, <https://doi.org/10.1007/s40820-023-01021-9>.
- [113] S. Wang, S. Zhao, X. Guo, G. Wang, 2D material-based heterostructures for rechargeable batteries, *Adv. Energy Mater.* 12 (4) (2022), 2100864, <https://doi.org/10.1002/aenm.202100864>.
- [114] L. Chen, Y. Wang, Y. Meng, F. Dou, Z. An, P. Song, G. Chen, D. Zhang, Integrated structure of tin-based anodes enhancing high power density and long cycle life for lithium ion batteries, *ACS Appl. Energy Mater.* 3 (9) (2020) 9337–9347, <https://doi.org/10.1021/acsaem.0c01688>.
- [115] S. Wang, P. Xiong, X. Guo, J. Zhang, X. Gao, F. Zhang, X. Tang, P.H.L. Notten, G. Wang, A stable conversion and alloying anode for potassium-ion batteries: A combined strategy of encapsulation and confinement, *Adv. Funct. Mater.* 30 (27) (2020), 2001588, <https://doi.org/10.1002/adfm.202001588>.
- [116] M. Goktas, C. Bolli, E.J. Berg, P. Novák, K. Pollok, F. Langenhorst, M.V. Roeder, O. Lenchuk, D. Mollenhauer, P. Adelhelm, Graphite as cointercalation electrode for sodium-ion batteries: electrode dynamics and the missing solid electrolyte interphase (SEI), *Adv. Energy Mater.* 8 (16) (2018) 1702724, <https://doi.org/10.1002/aenm.201702724>.
- [117] Q. Han, S. Wang, Z. Jiang, X. Hu, H. Wang, Composite polymer electrolyte incorporating metal–organic framework nanosheets with improved electrochemical stability for all-solid-state Li metal batteries, *ACS Appl. Mater. Interfaces* 12 (18) (2020) 20514–20521, <https://doi.org/10.1021/acsmami.0c03430>.
- [118] W. Luo, L. Zhou, K. Fu, Z. Yang, J. Wan, M. Manno, Y. Yao, H. Zhu, B. Yang, L. Hu, A thermally conductive separator for stable Li metal anodes, *Nano Lett.* 15 (9) (2015) 6149–6154, <https://doi.org/10.1021/acs.nanolett.5b02432>.
- [119] D. Deng, C. Bai, F. Xue, J. Lei, P. Xu, M. Zheng, Q. Dong, Multifunctional ion-sieve constructed by 2D materials as an interlayer for Li–S batteries, *ACS Appl. Mater. Interfaces* 11 (12) (2019) 11474–11480, <https://doi.org/10.1021/acsmami.8b22660>.
- [120] B. Li, H. Xu, Y. Ma, S. Yang, Harnessing the unique properties of 2D materials for advanced lithium–sulfur batteries, *Nanoscale Horiz.* 4 (1) (2019) 77–98, <https://doi.org/10.1039/C8NH00170G>.
- [121] F. Chu, J. Hu, C. Wu, Z. Yao, J. Tian, Z. Li, C. Li, Metal–organic frameworks as electrolyte additives to enable ultrastable plating/stripping of Li anode with dendrite inhibition, *ACS Appl. Mater. Interfaces* 11 (4) (2019) 3869–3879, <https://doi.org/10.1021/acsmami.8b17924>.
- [122] Q. Liu, R. Liu, Y. Cui, M. Zhou, J. Zeng, B. Zheng, S. Liu, Y. Zhu, D. Wu, Dendrite-free and long-cycling lithium metal battery enabled by ultrathin, 2D shield-defensive, and single lithium-ion conducting polymeric membrane, *Adv. Mater.* 34 (33) (2022), 2108437, <https://doi.org/10.1002/adma.202108437>.
- [123] Z. Li, I. Sami, J. Yang, J. Li, R.V. Kumar, M. Chhowalla, Lithiated metallic molybdenum disulfide nanosheets for high-performance lithium–sulfur batteries, *Nat. Energy* 8 (1) (2023) 84–93, <https://doi.org/10.1038/s41560-022-01175-7>.
- [124] M. Han, Y. Mu, J. Guo, L. Wei, L. Zeng, T. Zhao, Monolayer  $\text{MoS}_2$  fabricated by *in situ* construction of interlayer electrostatic repulsion enables ultrafast ion transport in lithium-ion batteries, *Nano-Micro Lett.* 15 (1) (2023) 80, <https://doi.org/10.1007/s40820-023-01042-4>.
- [125] P. Chong, Z. Zhou, K. Wang, W. Zhai, Y. Li, J. Wang, M. Wei, The stabilizing of 1T- $\text{MoS}_2$  for all-solid-state lithium-ion batteries, *Batteries* 9 (1) (2022), <https://doi.org/10.3390/batteries9010026>.
- [126] K.Y. Yang, H.T. Nguyen, Y.M. Tsao, S.B. Artemkina, V.E. Fedorov, C.W. Huang, H. C. Wang, Large area  $\text{MoS}_2$  thin film growth by direct sulfurization, *Sci. Rep.* 13 (1) (2023) 8378, <https://doi.org/10.1038/s41598-023-35596-5>.
- [127] G. Zhang, H. Liu, J. Qu, J. Li, Two-dimensional layered  $\text{MoS}_2$ : Rational design, properties and electrochemical applications, *Energy Environ. Sci.* 9 (4) (2016) 1190–1209, <https://doi.org/10.1039/c5ee03761a>.
- [128] R. Tilmann, C. Bartlam, O. Hartwig, B. Tywoniuk, N. Dominik, C.P. Cullen, L. Peters, T. Stimpel Lindner, N. McEvoy, G.S. Duesberg, Identification of ubiquitously present polymeric adlayers on 2D transition metal dichalcogenides, *ACS Nano* 17 (11) (2023) 10617–10627, <https://doi.org/10.1021/acsnano.3c01649>.
- [129] J. Fu, P. Yu, N. Zhang, G. Ren, S. Zheng, W. Huang, X. Long, H. Li, X. Liu, In situ formation of a bifunctional interlayer enabled by a conversion reaction to initiatively prevent lithium dendrites in a garnet solid electrolyte, *Energy Environ. Sci.* 12 (4) (2019) 1404–1412, <https://doi.org/10.1039/c8ee03390k>.

- [130] M.S. Kim, S.H. Deepika, M.S. Lee, J.H. Kim, K.R. Ryu, L.A. Lee, W.I.C. Archer, Enabling reversible redox reactions in electrochemical cells using protected LiAl intermetallics as lithium metal anodes, *Sci. Adv.* 5 (10) (2019), eaax5587, <https://doi.org/10.1126/sciadv.aax5587>.
- [131] A. Kizilaslan, T. Çetinkaya, H. Akbulut, 2H-MoS<sub>2</sub> as an artificial solid electrolyte interface in all-solid-state lithium–sulfur batteries, *Adv. Mater. Interfaces* 7 (20) (2020), 2001020, <https://doi.org/10.1002/admi.202001020>.
- [132] C. Huang, Z. Li, S. Duan, S. Xie, S. Yuan, S. Hou, G. Cao, H. Jin, Improving the stability of NASICON-type electrolyte with Li metal anode by interfacial modification, *J. Power Sources* 536 (2022), 231491, <https://doi.org/10.1016/j.jpowsour.2022.231491>.
- [133] E. Cha, H. Lee, W. Choi, Improving lithium-metal battery performance under the conditions of lean electrolyte through MoS<sub>2</sub> coating, *ChemElectroChem* 7 (4) (2020) 890–892, <https://doi.org/10.1002/celc.201901735>.
- [134] X. Yang, X. Gao, S. Mukherjee, K. Doyle Davis, J. Fu, W. Li, Q. Sun, F. Zhao, M. Jiang, Y. Hu, H. Huang, L. Zhang, S. Lu, R. Li, T.K. Sham, C.V. Singh, X. Sun, Phase evolution of a prenucleator for fast Li nucleation in all-solid-state lithium batteries, *Adv. Energy Mater.* 10 (37) (2020) 2001191, <https://doi.org/10.1002/aenm.202001191>.
- [135] W. Ren, W. Ma, S. Zhang, B. Tang, Recent advances in shuttle effect inhibition for lithium sulfur batteries, *Energy Storage Mater.* 23 (2019) 707–732, <https://doi.org/10.1016/j.ensm.2019.02.022>.
- [136] Z.A. Ghazi, X. He, A.M. Khattak, N.A. Khan, B. Liang, A. Iqbal, J. Wang, H. Sin, L. Li, Z. Tang, MoS<sub>2</sub>/Celgard separator as efficient polysulfide barrier for long-life lithium-sulfur batteries, *Adv. Mater.* 29 (21) (2017), 1606817, <https://doi.org/10.1002/adma.201606817>.
- [137] X. Yu, G. Zhou, Y. Cui, Mitigation of shuttle effect in Li-S battery using a self-assembled ultrathin molybdenum disulfide interlayer, *ACS Appl. Mater. Interfaces* 11 (3) (2019) 3080–3086, <https://doi.org/10.1021/acsami.8b19354>.
- [138] P. Guo, D. Liu, Z. Liu, X. Shang, Q. Liu, D. He, Dual functional MoS<sub>2</sub>/graphene interlayer as an efficient polysulfide barrier for advanced lithium-sulfur batteries, *Electrochimica Acta* 256 (2017) 28–36, <https://doi.org/10.1016/j.electacta.2017.10.003>.
- [139] A.G. Olabi, M.A. Abdulkareem, T. Wilberforce, E.T. Sayed, Application of graphene in energy storage device—A review, *Renew. Sustain. Energy Rev.* 135 (2021) 110026, <https://doi.org/10.1016/j.rser.2020.110026>.
- [140] Y. Li, Y. Li, Y. Yang, Z. Cui, J. Wang, T. Zhang, Conversion inorganic interlayer of a LiF/graphene composite in all-solid-state lithium batteries, *Chem. Commun.* 56 (11) (2020) 1725–1728, <https://doi.org/10.1039/c9cc09318d>.
- [141] A. Jiríčková, O. Jankovský, Z. Sofer, D. Sedmidubský, Synthesis and applications of graphene oxide, *Materials* 15 (3) (2022) 920, <https://doi.org/10.3390/ma15030920>.
- [142] T. Foroozan, F.A. Soto, V. Yurkiv, S. Sharifi Asl, R. Deivanayagam, Z. Huang, R. Rojace, F. Mashayek, P.B. Balbuena, R. Shahbazian Yassar, Synergistic effect of graphene oxide for impeding the dendritic plating of Li, *Adv. Funct. Mater.* 28 (15) (2018) 1705917, <https://doi.org/10.1002/adfm.201705917>.
- [143] W. Jia, Z. Li, Z. Wu, L. Wang, B. Wu, Y. Wang, Y. Cao, J. Li, Graphene oxide as a filler to improve the performance of PAN-LiClO<sub>4</sub> flexible solid polymer electrolyte, *Solid State Ion.* 315 (2018) 7–13, <https://doi.org/10.1016/j.ssi.2017.11.026>.
- [144] Z. Zhuang, L. Yang, B. Ju, A. Yin, G. Lei, Q. Zhou, Y. Tang, Z. Deng, F. Tu, S. Qin, Engineering LiNi<sub>0.5</sub>Co<sub>0.2</sub>Mn<sub>0.3</sub>O<sub>2</sub>/poly(propylene carbonate) interface by graphene oxide modification for all-solid-state lithium batteries, *Energy Storage* 2 (2) (2020), e109, <https://doi.org/10.1002/est2.109>.
- [145] S. Gomari, M. Esfandeh, I. Ghasemi, All-solid-state flexible nanocomposite polymer electrolytes based on poly(ethylene oxide): Lithium perchlorate using functionalized graphene, *Solid State Ion.* 303 (2017) 37–46, <https://doi.org/10.1016/j.ssi.2017.02.005>.
- [146] P. Zhai, Z. Yang, Y. Wei, X. Guo, Y. Gong, Two-dimensional fluorinated graphene reinforced solid polymer electrolytes for high-performance solid-state lithium batteries, *Adv. Energy Mater.* 12 (42) (2022), 2200967, <https://doi.org/10.1002/aenm.202200967>.
- [147] S. Roy, X. Zhang, A.B. Puthirath, A. Meiyazhagan, S. Bhattacharyya, M. M. Rahman, G. Babu, S. Susarla, S.K. Saju, M.K. Tran, Structure, properties and applications of two-dimensional hexagonal boron nitride, *Adv. Mater.* 33 (44) (2021), 2101589, <https://doi.org/10.1002/adma.202101589>.
- [148] X. Xu, L. Wang, H. Fei, L. Ci, Boron nitride doped Li<sub>x</sub>P<sub>2</sub>S<sub>11</sub> solid electrolyte with improved interfacial compatibility and application in all-solid-state Li/S battery, *J. Mater. Sci.: Mater. Electron.* 30 (21) (2019) 19119–19125, <https://doi.org/10.1007/s10854-019-02267-z>.
- [149] Z. Zhang, R.G. Antonio, K.L. Choy, Boron nitride enhanced polymer/salt hybrid electrolytes for all-solid-state lithium ion batteries, *J. Power Sources* 435 (2019), 226736, <https://doi.org/10.1016/j.jpowsour.2019.226736>.
- [150] K. Yan, H.W. Lee, T. Gao, G. Zheng, H. Yao, H. Wang, Z. Lu, Y. Zhou, Z. Liang, Z. Liu, S. Chu, Y. Cui, Ultrathin two-dimensional atomic crystals as stable interfacial layer for improvement of lithium metal anode, *Nano Lett.* 14 (10) (2014) 6016–6022, <https://doi.org/10.1021/nl503125u>.
- [151] Y. Li, L. Zhang, Z. Sun, G. Gao, S. Lu, M. Zhu, Y. Zhang, Z. Jia, C. Xiao, H. Bu, K. Xi, S. Ding, Hexagonal boron nitride induces anion trapping in a polyethylene oxide-based solid polymer electrolyte for lithium dendrite inhibition, *J. Mater. Chem. A* 8 (19) (2020) 9579–9589, <https://doi.org/10.1039/d0ta03677c>.
- [152] X. Yin, L. Wang, Y. Kim, N. Ding, J. Kong, D. Safanama, Y. Zheng, J. Xu, D.V. M. Repaka, K. Hippalgaonkar, S.W. Lee, S. Adams, G.W. Zheng, Thermal conductive 2D boron nitride for high-performance all-solid-state lithium-sulfur batteries, *Adv. Sci.* 7 (19) (2020), 2001303, <https://doi.org/10.1002/ads.202001303>.
- [153] H. An, Q. Liu, J. An, S. Liang, X. Wang, Z. Xu, Y. Tong, H. Huo, N. Sun, Y. Wang, Y. Shi, J. Wang, Coupling two-dimensional fillers with polymer chains in solid polymer electrolyte for room-temperature dendrite-free lithium-metal batteries, *Energy Storage Mater.* 43 (2021) 358–364, <https://doi.org/10.1016/j.ensm.2021.09.019>.
- [154] X. Li, Z. Huang, C.E. Shuck, G. Liang, Y. Gogotsi, C. Zhi, MXene chemistry, electrochemistry and energy storage applications, *Nat. Rev. Chem.* 6 (6) (2022) 389–404, <https://doi.org/10.1038/s41570-022-00384-8>.
- [155] M. Naguib, M. Kurtoglu, V. Presser, J. Lu, J. Niu, M. Heon, L. Hultman, Y. Gogotsi, M.W. Barsoum, Two-dimensional nanocrystals produced by exfoliation of Ti<sub>3</sub>AlC<sub>2</sub>, *Adv. Mater.* 23 (37) (2011) 4248–4253, <https://doi.org/10.1002/adma.201102306>.
- [156] Q. Man, Y. An, H. Shen, C. Wei, X. Zhang, Z. Wang, S. Xiong, J. Feng, MXenes and their derivatives for advanced solid-state energy storage devices, *Adv. Funct. Mater.* 33 (2023), 2303668, <https://doi.org/10.1002/adfm.202303668>.
- [157] J. Nan, X. Guo, J. Xiao, X. Li, W. Chen, W. Wu, H. Liu, Y. Wang, M. Wu, G. Wang, Nanoengineering of 2D MXene-based materials for energy storage applications, *Small* 17 (9) (2021), e1902085, <https://doi.org/10.1002/smll.201902085>.
- [158] C. Wei, Y. Tao, Y. An, Y. Tian, Y. Zhang, J. Feng, Y. Qian, Recent advances of emerging 2D MXene for stable and dendrite-free metal anodes, *Adv. Funct. Mater.* 30 (45) (2020), 2004613, <https://doi.org/10.1002/adfm.202004613>.
- [159] Q. Pan, Y. Zheng, S. Kota, W. Huang, S. Wang, H. Qi, S. Kim, Y. Tu, M. W. Barsoum, C.Y. Li, 2D MXene-containing polymer electrolytes for all-solid-state lithium metal batteries, *Nanoscale Adv.* 1 (1) (2019) 395–402, <https://doi.org/10.1039/c8na00206a>.
- [160] S. Ha, D. Kim, H.K. Lim, C.M. Koo, S.J. Kim, Y.S. Yun, Lithiophilic MXene-guided lithium metal nucleation and growth behavior, *Adv. Funct. Mater.* 31 (32) (2021), 2101261, <https://doi.org/10.1002/adfm.202101261>.
- [161] V. Vijayakumar, M. Ghosh, K. Asokan, S.B. Sukumaran, S. Kurungot, J. Mindemark, D. Brandell, M. Winter, J.R. Nair, 2D layered nanomaterials as fillers in polymer composite electrolytes for lithium batteries, *Adv. Energy Mater.* 13 (15) (2023), 2203326, <https://doi.org/10.1002/aenm.202203326>.
- [162] Y. Hou, Z. Huang, Z. Chen, X. Li, A. Chen, P. Li, Y. Wang, C. Zhi, Bifunctional separators design for safe lithium-ion batteries: Suppressed lithium dendrites and fire retardance, *Nano Energy* 97 (2022), 107204, <https://doi.org/10.1016/j.nanoen.2022.107204>.
- [163] Y. Liu, J. Zhang, X. Zhang, Y. Li, J. Wang, Ti<sub>3</sub>C<sub>2</sub>T<sub>x</sub> filler effect on the proton conduction property of polymer electrolyte membrane, *ACS Appl. Mater. Interfaces* 8 (31) (2016) 20352–20363, <https://doi.org/10.1021/acsm.6b04800>.
- [164] X. Meng, Y. Liu, M. Guan, J. Qiu, Z. Wang, A high-energy and safe lithium battery enabled by solid-state redox chemistry in a fireproof gel electrolyte, *Adv. Mater.* 34 (28) (2022), e2201981, <https://doi.org/10.1002/adma.202201981>.
- [165] Q. Zhao, Q. Zhu, Y. Liu, B. Xu, Status and prospects of MXene-based lithium-sulfur batteries, *Adv. Funct. Mater.* 31 (21) (2021), 2100457, <https://doi.org/10.1002/adfm.202100457>.
- [166] D. Wang, F. Li, R. Lian, J. Xu, D. Kan, Y. Liu, G. Chen, Y. Gogotsi, Y. Wei, A general atomic surface modification strategy for improving anchoring and electrocatalysis behavior of Ti<sub>3</sub>C<sub>2</sub>T<sub>x</sub> MXene in lithium-sulfur batteries, *ACS Nano* 13 (10) (2019) 11078–11086, <https://doi.org/10.1021/acsnano.9b03412>.
- [167] L. Jiao, C. Zhang, C. Geng, S. Wu, H. Li, W. Lv, Y. Tao, Z. Chen, G. Zhou, J. Li, G. Ling, Y. Wan, Q.H. Yang, Capture and catalytic conversion of polysulfides by in situ built TiO<sub>2</sub>-MXene heterostructures for lithium-sulfur batteries, *Adv. Energy Mater.* 9 (19) (2019), 1900219, <https://doi.org/10.1002/aenm.201900219>.
- [168] T. Qin, Z. Wang, Y. Wang, F. Besenbacher, M. Otyepka, M. Dong, Recent progress in emerging two-dimensional transition metal carbides, *Nanomicro Lett.* 13 (1) (2021) 183, <https://doi.org/10.1007/s40820-021-00710-7>.
- [169] Z. Sun, Y. Li, S. Zhang, L. Shi, H. Wu, H. Bu, S. Ding, g-C<sub>3</sub>N<sub>4</sub> nanosheets enhanced solid polymer electrolytes with excellent electrochemical performance, mechanical properties, and thermal stability, *J. Mater. Chem. A* 7 (18) (2019) 11069–11076, <https://doi.org/10.1039/c9ta00634f>.